http://pubs.acs.org/journal/acsodf
Article

Implications of Organic Matter Input, Sedimentary Environmental Conditions, and Gas Generation Potential of the Organic-Rich Shale in the Onshore Jiza-Qamar Basin, Yemen

Mohammed Hail Hakimi,* Ali Kahal, Afikah Rahim,* Waqas Naseem, Wedad Alsomid, Alia Al-Buraihi, Thoraia Alyousofi, Shuaib Alqahtani, Hesham AbdulAziz Alyousofi, and Naira Magdy Lotfy

Cite This: ACS Omega 2023, 8, 30483−30499

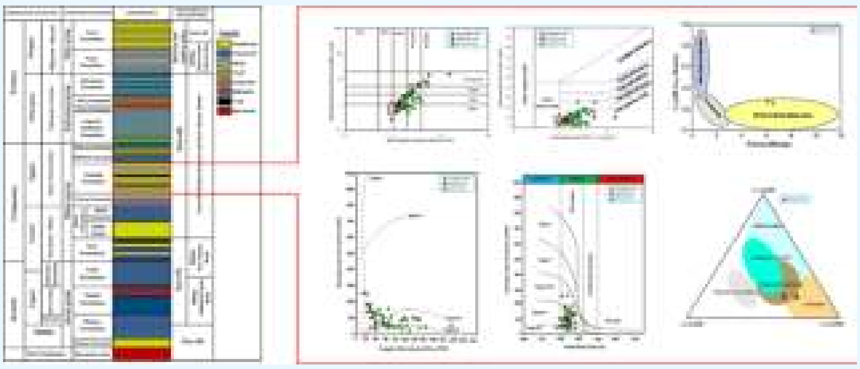

ABSTRACT: The Jiza-Qamar Basin is one of the most important exploration sedimentary basins in Yemen. For over a decade, the exploration of hydrocarbons has been occurring in this basin. Late Cretaceous age rocks are the most occurring organic-rich sediments in this basin, including coals, coaly shales, and shales. The studied organic-rich shale beds are from the Late Cretaceous Mukalla Formation and associated with coal seams. These organic-rich shales can serve as source rocks for hydrocarbon generation potential. The current study investigates the geochemical characteristics, including assessing the organic matter (OM) input, sedimentary environmental conditions, and hydrocarbon generation potential of the organic-rich shale within the Mukalla Formation from three well locations in the onshore Jiza-Qamar Basin using organic geochemistry, biomarker, and carbon isotope measurements. The studied shale samples have high OM content with total organic carbon values between 0.74 and 19.48 wt %. Furthermore, they contain mainly hydrogen-poor Types III and IV kerogen, indicating the presence of the gas-prone source rock. The presence of these types of kerogen indicates the abundance of vitrinite and inertinite macerals, as established by microscopic investigation. However, the studied organic-rich shales had biomarker features, including high Ph/Ph ratio between 3.82 and 7.46, high Tm/Ts ratio of more than 7, and high C_{29} regular steranes compared to C_{27} and C_{28} regular steranes. Apart from the biomarker results, the studied Mukalla shales are characterized by the abundance of land-derived OM that deposited in fluvial to fluvial deltaic environments under highly oxic conditions. The finding of the considerable concentration of terrigenous OM is probably confirmed by the bulk carbon isotope and maceral composition data. The maturity indicators show that the examined organic-rich shale samples in the studied wells exhibit low VR values of up to 0.71%, and thereby, they have not been yet reached the high maturity for gas generation. This low maturity level in the studied wells is probably attributed to shallow burial depth, exhibiting depth of up to 2835 m. Therefore, the substantial gas exploration operations from the organic-rich shale source rock system of the Late Cretaceous Mukalla Formation can be recommended in the deeper stratigraphic succession in the offshore Jiza-Qamar Basin.

1. INTRODUCTION

Organic-rich sediments such as oil shale and gas shale are the key hydrocarbon resources worldwide and have recently become important global exploration targets.[1,2] These fine-grained sedimentary rocks are of great interest owing to their organic-rich matter and have drawn attention as a source rock for conventional and unconventional gas and oil over the past 30 years.[2−4] However, both marine and continental organic-rich

Received: May 25, 2023
Accepted: July 19, 2023
Published: August 10, 2023

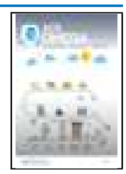

https://doi.org/10.1021/acsomega.3c03691
ACS Omega 2023, 8, 30483−30499

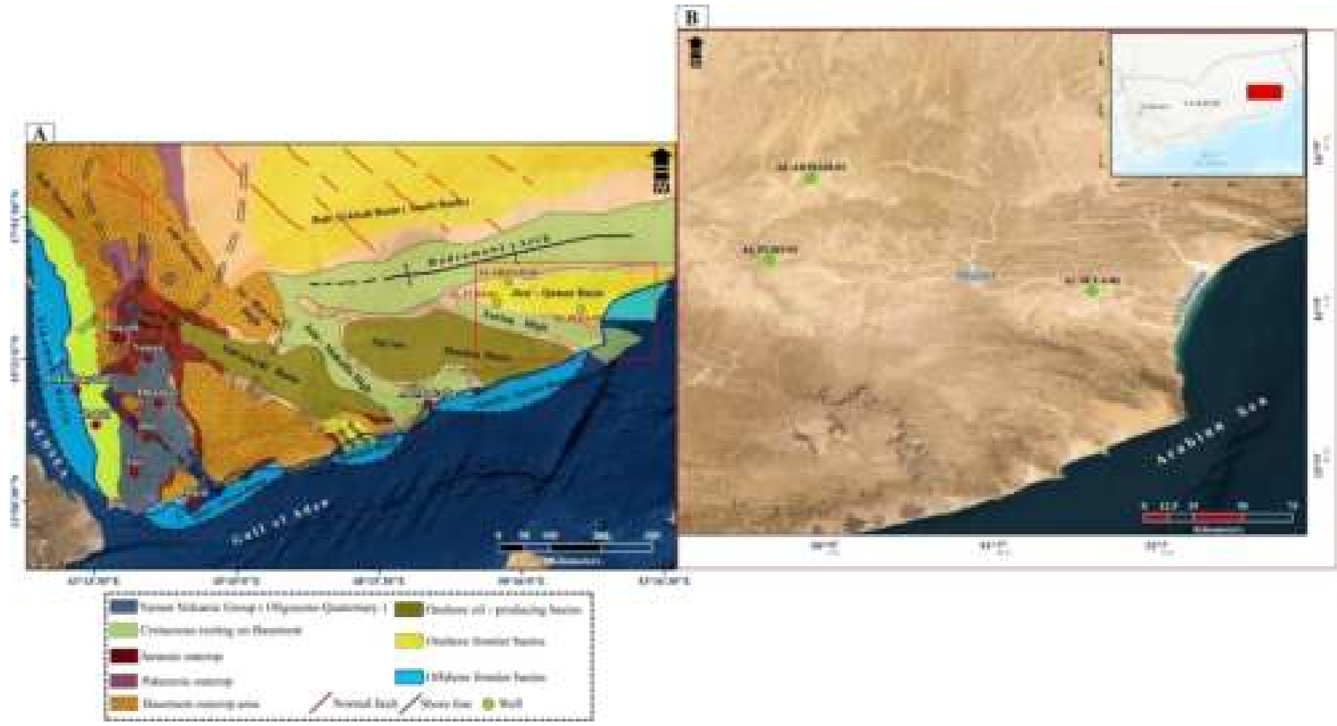

Figure 1. (A) Main sedimentary basins in the Republic of Yemen and (B) location map of the three studied wells (i.e., Al-Armah-01, Al-Furt-01, and Al-Jeza-01) in the onshore Jiza-Qamar Basin.

shale sediments have been successfully explored and developed worldwide, showing valuable source rocks for generation of significant amounts of hydrocarbon during thermal maturation, and they have been proved by several studies.[5−15]

The knowledge of geology, lithofacies, and organic matter (OM) characteristics of these organic-rich shales seriously limits gas and oil exploration in any sedimentary basin.[16−18] Apart from source rock characteristics and petroleum generative potential, multi-integrated techniques such as organic geochemistry, microscopic examination, combined with biomarker measurements are vital to the study of shale source rock systems and shed critical insights on the conventional as well as unconventional petroleum resource potential.[1,19,20]

The key focus of the present study is the Jiza-Qamar Basin, which lies mostly onshore and partly offshore in north eastern part of Yemen and is bounded to the north by the Hadramawt Arch, which separates this basin from the southern flank of the Rub' Al-Khali Basin (Figure 1A).

The Jiza-Qamar Basin contains a Middle Jurassic to Paleogene sedimentary fill up to 6 km thick.[21] The Late Cretaceous sediments across Jiza-Qamar Basin host a number of OM-rich strata, such as coals, coaly shales, and shales.[5−7,22] However, a number of researchers have assessed origin, paleodepositional conditions, and geochemical characteristics of OM, as well as the potential for petroleum generation potential of the coals, coaly shales of the Late Mukalla Formation from well locations in the offshore Jiza-Qamar basin and indicate that the coals, coaly shales, and shales of the Mukalla Formation are an important organic-rich facies and high-quality oil-and gas-prone source rocks for exploration, development, and production targets in the offshore Jiza-Qamar Basin.[5−7,22,23]

There have been few geochemical investigations of the organic-rich shale sediments found in the Late Cretaceous succession of the onshore portion of the Jiza-Qamar Basin. In this case, the current research focuses on the OM-bearing shale sediments, particularly those of the Mukalla Formation in the onshore Jiza-Qamar Basin (Figure 1B).

The goal of this research is to enhance our understanding of the source rock properties of the organic-rich shale rocks of the Mukalla Formation, which are of economic and scientific importance. An inclusive investigation of the large-scale characteristics of OM and the hydrocarbon potential of the organic-rich shale deposits from three well locations (Al-Armah-01, Al-Furt-01, and Al-Jeza-01) in the onshore part of the basin is conducted using integrated geochemical and organic petrographic methods. This study also attempts to integrate the biomarker measurements together with carbon isotope compositions and used to understand the source and origin OM inputs and their sedimentary environmental conditions during deposition of the organic-rich shale unit of the Mukalla Formation in the investigated onshore part of the basin. In addition, this research discusses the implications of hydrocarbon generation potential and thereby deciphers the hydrocarbon exploration and development in the basin.

2. GEOLOGICAL SETTING

The Jiza-Qamar Basin is an extensional rift basin, which is associated with the rifting mechanisms of the break-up of Gondwana during the Late Jurassic to Early Cretaceous.[21,24] The Jiza-Qamar Basin comprises both onshore and offshore segments (Figure 1A) and is characterized by horst-graben structures separated by highly dipping normal faults.[21]

The Jiza-Qamar Basin is filled with thick sedimentary succession, ranging in age between Mesozoic and Cenozoic, with several significant unconformities.[21] The lithostratigraphic column of the studied basin is presented in Figure 2. The Middle Jurassic pre-rift sediments were deposited unconformably above the Precambrian basement rocks (Figure 2). Clastics and carbonate sediments dominate the pre-rift succession. The

https://doi.org/10.1021/acsomega.3c03691
ACS Omega 2023, 8, 30483−30499

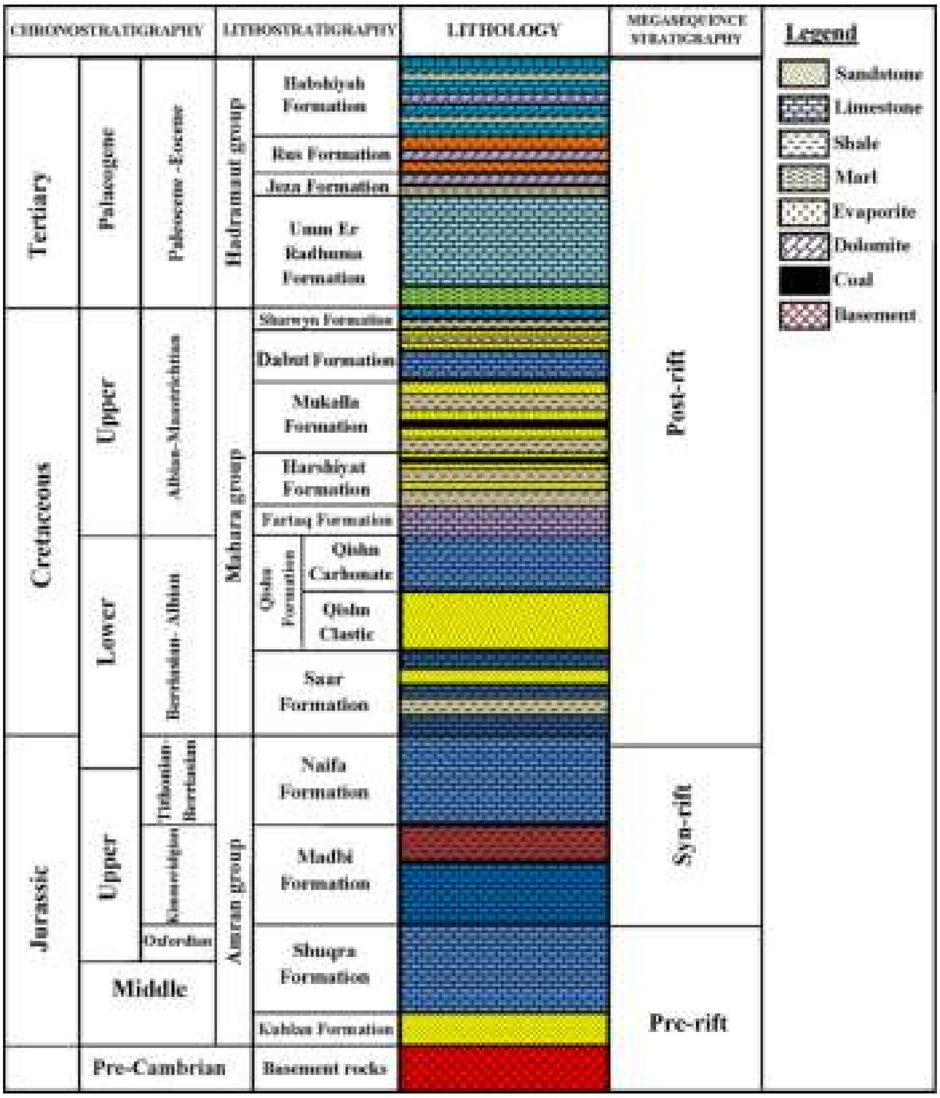

Figure 2. Stratigraphic column for the Jiza-Qamar Basin.

Middle Jurassic clastics of the Kuhlan Formation represent the early pre-rift sedimentation.[25] In contrast, the marine platform carbonates of the Shuqra Formation accumulated during the late pre-rift phase (Callovian-Oxfordian).

During the Kimmeridgian-Berriasian, a rifting phase is recognized[24,26,27] and includes thick carbonates and shales of the Madbi and Naifa formations (Figure 2). The shale units of the syn-rift Madbi Formation are source rocks with high oil generation potential in the Sab'atayn and Masilah hydrocarbon-producing basins.[28−31] The syn-rift deposits of the Madbi Formation and the lower part of Naifa Formation are followed by post-rift clastic and carbonate sediments (Figure 2). The post-rift sequence includes several formations of the Mahara and Hadramaut groups.[21] The Mahara Group contains mixed clastic and carbonate deposits, while the Hadramaut Group consists mainly of carbonates (Figure 2).

The Mukalla and Harshiyat formations of the Mahara Group are mostly composed of intercalations of sandstone, shale, and coal (Figure 2). The organic-rich (coal, coaly shale, and shale) successions of the Mahara Group (Mukalla and Harshiyat formations) are an important source rocks for exploration, development, and production targets in the basin.[5,22,23,32−34]

The key focus of the present study is on the formation of the Mahara Group, including Mukalla Formation. The Mukalla sediments are considered to have been deposited in deltaic and near-shore to offshore marine-shelf environments.[5] The marine depositional environments were deep enough for basinal facies of suboxic-anoxic character to accumulate and yield a mixture of marine palynomorphs (dinoflagellate cysts, acritarchs, and linings of foraminiferal tests) and terrestrially derived spores and pollen.[5] This formation was formed during the separation of Madagascar and India from southern Gondwana and the breaking up of southern Gondwana in the late Mesozoic.[35]

During the Late Cretaceous, the Mukalla and Harshiyat formations of the Mahara Group were also deposited in the Jiza-Qamar Basin and are mainly carbonates with intercalations of sandstone and shale (Figure 2). The Mahara Group, conformably overlain by the Hadramaut sediments, consists of mainly carbonate with intercalations of evaporite and shale (Figure 2). Paleogene formations (Paleocene-Eocene) of the Hadramaut Group are found in conformable contacts, such as the Umm Er Radhuma Formation (limestone and marl), Jeza Formation (dolomite and shale), Rus Formation (dolomite and evaporite), and Habshiyah Formation (limestone, dolomite, and shale), as shown in Figure 2.

https://doi.org/10.1021/acsomega.3c03691
ACS Omega 2023, 8, 30483−30499

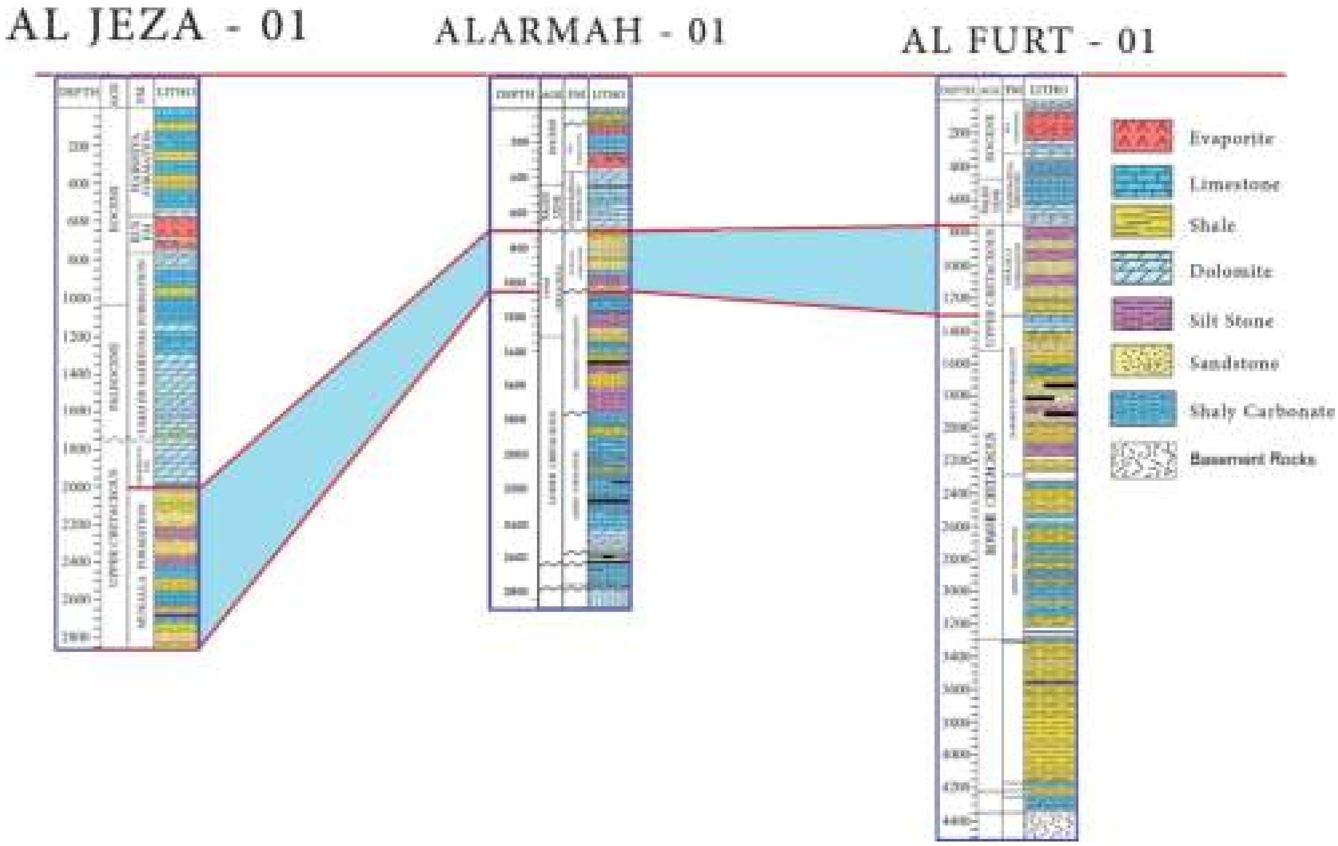

Figure 3. Lithostratigraphic logs of the three wells studied (i.e., Al-Armah-01, Al-Furt-01, and Al-Jeza-01) in the onshore Jiza-Qamar Basin.

3. MATERIALS AND EXPERIMENTAL METHODS

77 drill cutting samples were collected from the organic-rich shale facies of the Late Cretaceous Mukalla Formation in three well locations (Al-Armah-01; Al-Furt-01; and Al-Jeza-01 wells), as shown in Figure 3.

The collected samples were cleaned to remove contamination from the drilling mud and related additives (i.e., water-based drilling fluid) and were milled into ±18 mesh (approximate ≤1mm) and 72 mesh sizes using a mortar and pestle. These organic-rich shale samples were then subjected to multi geochemical methods along with optical microscopic studies. However, limited shale samples were selected for geochemical analyses (i.e., biomarker and carbon isotope) along with optical microscopic analysis because of the limitations of shale samples and analytical costs.

3.1. Organic Geochemical Examinations. Geochemical analyses, including the total organic carbon (TOC) content, Rock-Eval programmed pyrolysis, bitumen extraction, gas chromatography (GC) and gas chromatography-mass spectroscopy (GC−MS) analyses, as well as carbon isotope composition ($^{\delta 13}$C), were conducted on the Mukalla shale samples from the studied wells, and their OM compositions were measured.

The TOC measurement was performed on the studied 77 shale samples using a LECO CS125 system and measured in weight %. However, the crushed samples were treated to remove carbonate minerals with 10% diluted hydrochloric acid before determining the organic carbon content.

The programmed pyrolysis analysis was subsequently performed on 40 shale samples using a Rock Eval-II instrument. This analysis was carried out using a programmed oven temperature between 300 and 600 °C according to the procedure outlined by Espitalie et al.[36] and Lafargue et al.[37] After the heat treatment, three chromatographic peaks (S_1, S_2, and S_3) were generated, and the T_{max} values were determined (Table 1). The S_1 peak is indicative of the volatized hydrocarbons in the rock at 300 °C, the S_2 peak is assigned to the hydrocarbons generated from insoluble kerogen during heating from 300 to 600 °C, and the peak S_3 indicates the amount of CO_2 entrapped at 390 °C during the thermal alteration of the oxygenated organic compounds. T_{max} is the temperature at the S_2 peak, indicating the maximum hydrocarbon generation amount through the pyrolysis at a temperature between 300 and 600 °C; it is also an indicator of the OM maturity.

The following additional indices were calculated from the pyrolysis data: hydrogen index [HI = (S_2×100/TOC) mg HC/g TOC], oxygen index [OI = (S_3 × 100/TOC) mg CO_2/g TOC], and production index [PI = S_1/(S_1 + S_2) mg HC/g rock], following the studies of Peters and Cassa.[38]

Afterward, selected four shale samples from Al-Furt-01 and Al-Jeza-01 wells were subjected for bitumen extraction using Soxhlet-extracted for 72 h, with a mixture solvent (dichloromethane and acetone). The extracted bitumen fraction in these shale samples was broken down into their individual components, including aliphatic, aromatic, and polar components (NSO) using liquid column chromatography. In addition, the aliphatic fraction from the four shale samples was then analyzed using the GC system. The GC experiment was performed using a Hewlett Packard 5890, with the temperature rising at a rate of 3 °C per minute from 70 to 270 °C and then remaining constant at 270 °C for 30 min.

Later, the GC−MS was utilized to decipher the saturated hydrocarbon fraction within the selected two shale samples

https://doi.org/10.1021/acsomega.3c03691
ACS Omega 2023, 8, 30483−30499

Table 1. Geochemical Results of the Analyzed Organic-Rich Shale Samples within the Mukalla Formation from Three Exploration Well Locations (Al-Armah-01, Al-Furt-01, and Al-Jeza-01) in the Onshore Jiza-Qamar Basin, Eastern Yemen, Including TOC Content, Programmed Pyrolysis (Rock-Eval-II), Maceral Composition, and Vitrinite Reflectance (VRo %) Measurements[a]

				Rock-Eval pyrolysis data							maceral composition (wt. %)			
field	well	depth (m)	TOC Wt %	S_1-HC (mg/g)	S_2-HC (mg/g)	S_2-CO_2 (mg/g)	T_{max} (°C)	HI (mg/g)	OI (mg/g)	PI (mg/g)	liptinite	vitrinite	inertinite	vitrinite reflectance (VRo %)
Onshore Jiza -Qamar Basin	Al-Armah-01	717	4.17								30	65	5	0.39
		765	3.43											
		774	3.95	1.62	5.41	1.38	441	137	35	0.23				
		786	2.38	0.17	2.28	2.19	432	96	92	0.07				
		804	2.46	0.87	3.47	0.71	442	141	29	0.20				
		834	3.39	0.74	5.42	0.85	438	160	25	0.12				
		858	15.40	0.65	15.55	4.31	429	101	28	0.04				
		864	5.69	1.95	14.28	1.02	431	251	18	0.12				
		867	3.40	0.08	1.90	2.18	432	56	64	0.04				
		876	2.00	0.08	1.82	2.42	433	91	121	0.04				
		888	1.31	0.07	0.58	1.79	432	44	137	0.11	15	75	10	0.44
		894	1.81	0.44	2.33	0.58	442	129	32	0.16				
		924	0.98	0.54	1.21	0.43	445	123	44	0.31				
		933	3.00								15	75	10	0.43
		975	1.70	0.04	1.04	0.99	435	61	58	0.04				
		984	2.56	0.91	2.89	0.87	437	113	34	0.24				
		996	5.37	0.22	5.32	2.79	432	99	52	0.04				
		1014	3.23	0.59	6.01	0.65	442	186	20	0.09				
		1020	2.72	0.07	1.66	1.44	439	61	53	0.04	15	85	minor	0.40
		1044	0.94	0.12	0.28	0.36	445	30	38	0.30				
	Al-Furt-01	756	1.84	0.03	0.72	1.32	426	39	72	0.04				
		783	3.91	0.01	1.41	2.39	439	36	61	0.01				
		810	2.66	1.63	4.20	1.68	439	158	63	0.28				
		813	2.69	0.02	0.78	2.42	437	29	90	0.02				
		843	2.07	0.02	0.50	2.17	438	24	105	0.04				
		870	1.50											
		873	2.24	0.04	0.85	2.80	436	38	125	0.04				
		900	1.78	0.25	2.03	0.89	435	114	50	0.11				
		903	2.64	0.01	1.45	1.85	439	55	70	0.01				
		930	3.55	0.27	6.46	0.99	435	182	28	0.04				
		933	1.92	0.01	0.86	1.56	439	45	81	0.01				
		960	2.37	0.19	3.65	1.04	436	154	44	0.05				
		963	1.48	0.07	0.77	1.47	439	52	99	0.08				
		990	2.21	0.21	2.74	0.95	437	124	43	0.07				
		1020	1.42	0.63	1.41	1.68	440	99	118	0.31	10	85	5	0.42
		1053	0.92											
		1080	1.35	0.43	1.36	1.30	437	101	96	0.24				
		1083	1.05	0.06	0.56	1.97	440	53	188	0.1				
		1110	0.96											
		1113	1.55	0.05	0.81	1.33	429	52	86	0.06				
		1140	1.25	0.04	0.79	0.73	439	63	58	0.05				
		1143	0.94											
		1170	0.72											
		1203	2.73	0.06	3.03	0.87	435	111	32	0.02				
		1230	2.19	0.09	2.80	0.70	440	128	32	0.03				
		1233	1.84	0.04	1.18	0.81	441	64	44	0.03				
		1260	1.35											

				Rock-Eval pyrolysis data							Maceral composition (wt %)		
field	well	depth (m)	TOC wt %	S_1-HC (mg/g)	S_2-HC (mg/g)	S_2-CO_2 (mg/g)	T_{max} (°C)	HI (mg/g)	OI (mg/g)	PI (mg/g)	liptinite	vitrinite	inertinite
Onshore Jiza -Qamar Basin	Al-Jeza -01	2045	1.58										
		2141	4.00										

https://doi.org/10.1021/acsomega.3c03691
ACS Omega 2023, 8, 30483−30499

Table 1. continued

				Rock-Eval pyrolysis data							Maceral composition (wt %)			
field	well	depth (m)	TOC wt %	S_1-HC (mg/g)	S_2-HC (mg/g)	S_2−CO_2 (mg/g)	T_{max} (°C)	HI (mg/g)	OI (mg/g)	PI (mg/g)	liptinite	vitrinite	inertinite	
		2142	4.65	0.09	8.51	1.02	434	183	22	0.01	10	90	minor	0.45
		2235	1.04											
		2265	1.34											
		2271	1.30	0.07	1.27	1.63	436	98	125	0.05				
		2295	0.95											
		2307	1.35	0.03	1.27	1.32	438	94	98	0.02	minor	100	minor	0.52
		2325	1.61		2.24	0.34	445	139	21					
		2355	2.42	0.06	6.27	0.29	438	259	12	0.01				
		2385	1.77											
		2406	1.18	0.03	0.96	0.61	439	81	52	0.03				
		2415	1.03											
		2418	0.80	0.08	0.84	0.89	434	105	111	0.09				
		2565	0.74											
		2610	0.83	0.03	0.51	0.45	438	61	54	0.06				
		2670	1.43	0.08	1.24	0.53	440	87	37	0.06	5	90	5	0.52
		2685	1.52	0.03	0.78	0.53		51	35	0.04				
		2715	1.41	0.06	1.00	0.51	446	71	36	0.06				
		2718	1.22	0.05	1.09	1.07	438	89	88	0.04				
		2730	1.10	0.04	0.90	0.69	438	82	63	0.04	minor	95	5	0.51
		2745	1.18	0.03	0.52	0.32		44	27	0.05				
		2775	1.68	0.05	1.75	0.45	453	104	27	0.03				
		2778	1.38	0.10	1.53	0.94	436	111	68	0.06	minor	95	5	0.50
		2805	19.48											
		2814	5.30	0.44	8.27	1.33	435	156	25	0.05				
		2835	10.34								minor	100	minor	0.71

[a]TOC = total organic carbon; S_1-peak = free contents of hydrocarbon(mg HC/g rock); S_2-peak = remaining hydrocarbon potential (mg HC/g rock); S_3 peak = produced carbon dioxide (mg CO_2/g rock); HI = $S_2 \times 100$/TOC (mg HC/g rock); OI = $S_3 \times 100$/TOC (mg CO_2/g TOC); T_{max} = maximum temperature at peak of S_2(°C); and PI = production index $[S_1/(S_1 + S_2)]$.

using Hewlett Packard MSD with a 30/60 DB5-MS column. The GC−MS furnace consisted of a capillary column which is 30 m long and 0.32 mm in diameter, and the samples were warmed from 60 to 300 °C, at a rate of 3 °C/min rate, and carried out through the GC line operating at 300 °C for 20 min. As a result, the lipid compounds within the saturated HC fraction, i.e., hopanoids, terpanes, and steranes, were produced and analyzed based on the peak heights from m/z 191 and 217 mass fragmentograms, respectively.

Bulk $^{\delta13}$C composition facility was obtained from the geochemical laboratories of Simon Petroleum Technology Limited, United Kingdom. This analysis was carried out on the aliphatic and aromatic fractions from two shale samples using a VG 602 mass spectrometer. The $^{13}C/^{12}C$ isotope ratio of the saturate and aromatic HC fractions was determined using the combustion technique of Sofer and a Finnigan Delta E isotope ratio mass spectrometer.[39] The results are calibrated against the Pee Dee Belemnite standard.

3.2. Organic Petrology. Organic petrographic examinations, including the maceral content and reflectance measurement, were performed on the 11 shale samples using a standard polished block method.[40] The entire shale samples were pulverized into tiny pieces (around 1.5−2 mm, pea sized) and then inserted into molds using a SeriFix resin with cold-mount hardener combination. The blocks were polished after hardening to expose the sample's surface. Then, using silicon carbide paper and alumina powder, those were singly polished to smooth the surfaces following ASTM D2797-04.

The polished blocks of the shale samples immersed in oil under white plane-polarized reflected light, which enabled a good measurement of the vitrinite reflectance (VRo). The percentage of vitrinite reflectance (% VRo) was measured after calibration using a Zeiss microscope and Leitz Orthoplan/MPV photometry system, and the mean of reflectance values were calculated from more than 40 measurements per sample.

In addition, the polished blocks of the 11 shale samples immersed in oil were examined for the type of maceral and differentiation of its assemblages.

4. RESULTS

4.1. Organic Petrology. Organic petrology has been characterized by microscopic investigation and used to measure the % VRo under plane-polar reflected light. The results show that the analyzed shales in the studied wells exhibit VR range between 0.39 and 0.71% (Table 1), indicating immature to early mature oil generation window (Figure 4).

The Mukalla shale samples from the wells Al-Armah-01 and Al-Furt-01 reached shallow burial depths of less than 1300 m (Figure 3), which is congruent with the immature stage, exhibiting VRo values between 0.39 and 0.44% (Figure 4). In contrast, the shale samples from Al-Jeza-01 well were collected from depths between 2000 and 2800 m (Figure 3) and attained a different degree of thermal maturity (Figure 4), ranging from immature to the early mature oil generation window (Figure 4). Samples between 2300 and 2800 m from this studied well exhibit relatively higher maturity level of the early mature oil generation window (Figure 4). The relatively high maturity level is possibly because of the burial temperature at the relatively deep burial depths of more than 2300 m (Figure 4).

https://doi.org/10.1021/acsomega.3c03691
ACS Omega 2023, 8, 30483−30499

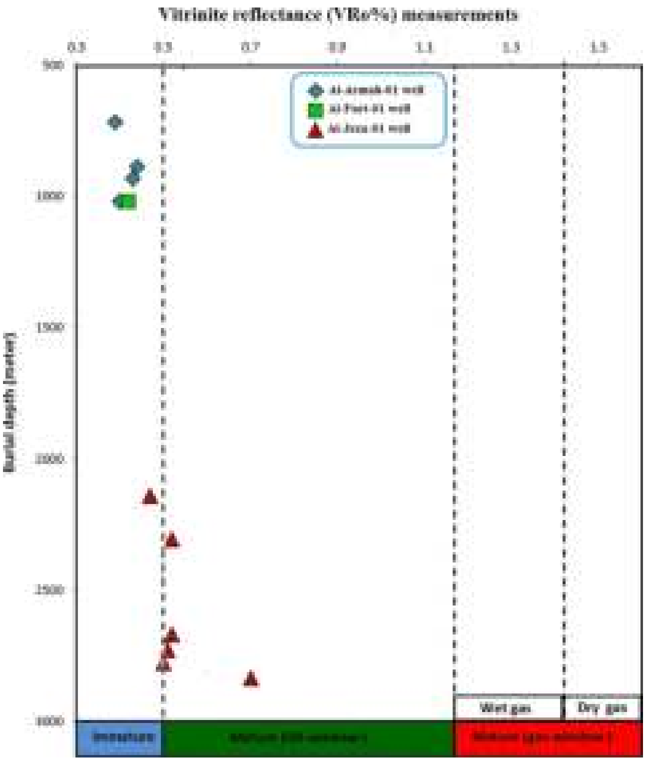

Figure 4. Distributions of the measured VRo via burial depth in the studied wells, showing that the analyzed Mukalla shale samples have different thermal maturity, ranking from immature to early mature oil generation window.

In addition, the maceral composition was also performed on the studied 11 shale samples using microscopic investigation under plane-polar reflected light. The overall composition of the macerals was determined based on free mineral matter, with the observations being presented in Table 1. The results show that the studied Mukalla shales have a high abundance of the vitrinite maceral, derived from terrestrial OM of up to 100% (Table 1). In contrast, liptinitic and inertinite macerals are represented in minor amounts, ranging from 5 to 30% and 5 to 10%, respectively (Table 1).

4.2. TOC and Rock-Eval Pyrolysis Results. The geochemical results of the Mukalla shale samples in the studied wells, including the TOC content and several parameters of S_1, S_2, S_3, HI, OI, and PI obtained from the Rock-Eval pyrolysis, are summarized in Table 1.

The measured TOC contents of all the studied shale samples in the Mukalla Formation exhibit values in the range of 0.74−19.48 wt % (Table 1). Most of the measurements indicate a TOC content of >1 wt % (1.03−19.48 wt %), whereas other samples exhibited a lower TOC content of 0.74−0.96 wt %, as shown in Table 1.

The petroleum yield of S_2 was generated during the programmed pyrolysis and generally consistent with TOC contents (Figure 5a). The S_2 values range between 0.28 and 15.55 (Table 1). Most of the samples have lower S_2 yields, ranging between 0.28 and 4.24 mg HC/g rock (Table 1), whereas the remaining 10 samples exhibit S_2 values of >5 mg HC/g rock (5.32−15.55 mg HC/g rock), as shown in Table 1. Moreover, the S_2 generation of most of the analyzed shale samples was found to be more than 1. Therefore, the most reliable Rock-Eval T_{max} value was determined to be between values of 429 and 453 °C (Table 1).

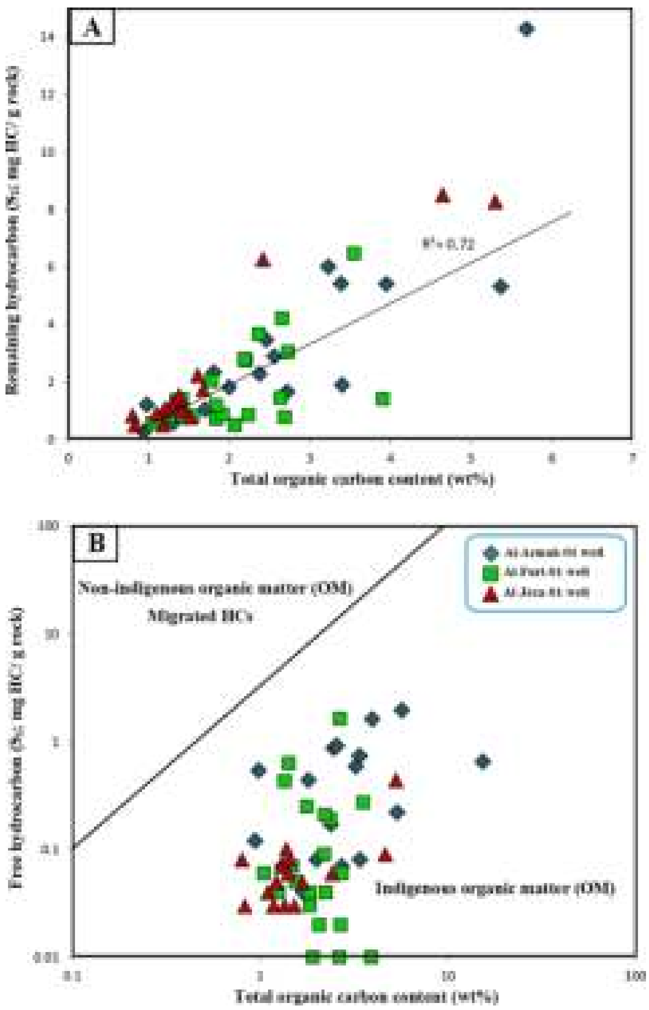

Figure 5. Geochemical correlations between (A) TOC content versus Rock-Eval pyrolysis (S_2) and (B) TOC content versus Rock-Eval pyrolysis (S_1) for the analyzed organic-rich shale samples of the Mukalla Formation in the studied wells, implying that these shales exhibit good petroleum generation potential and contain mainly indigenous OM.

Conversely, the pyrolysis data revealed that the free petroleum (S_1) yields in most of the examined shale samples are smaller, ranging from 0.01 to 1.95 mg hydrocarbon/g rock (Table 1). The low values of free hydrocarbon yields (S_1) may suggest that the Mukalla shales from the studied wells are still in the low mature level and mainly consist indigenous OM, as seen in the TOC-S_1 cross-plot (Figure 5b).

In this study, hydrogen, oxygen, and production indices were also obtained based on the S_1, S_2, and S_3 yields (see Table 1). However, the HI values of the shale samples under consideration were calculated by the combination between the S_2 yielded from pyrolysis and TOC contents and show range between 24 and 259 mg HC/g TOC (Table 1). Most of the shale samples exhibit HI values of <200 mg HC/g TOC (24−186), whereas other two samples show the highest HI values between 251 and 259 mg HC/g TOC (Table 1).

In addition, the amount of CO_2 released during the pyrolysis of the oxygenated organic compounds (S_3 peak) was in the range of 0.29−4.31 mg CO_2/g rock (Table 1). The S_3 values were also compared with TOC contents and used to calculate the OI. The OI values of the studied shale samples range from 12 mg CO_2/g TOC to 188 mg CO_2/g TOC (Table 1). Most of the shale

https://doi.org/10.1021/acsomega.3c03691
ACS Omega 2023, 8, 30483−30499

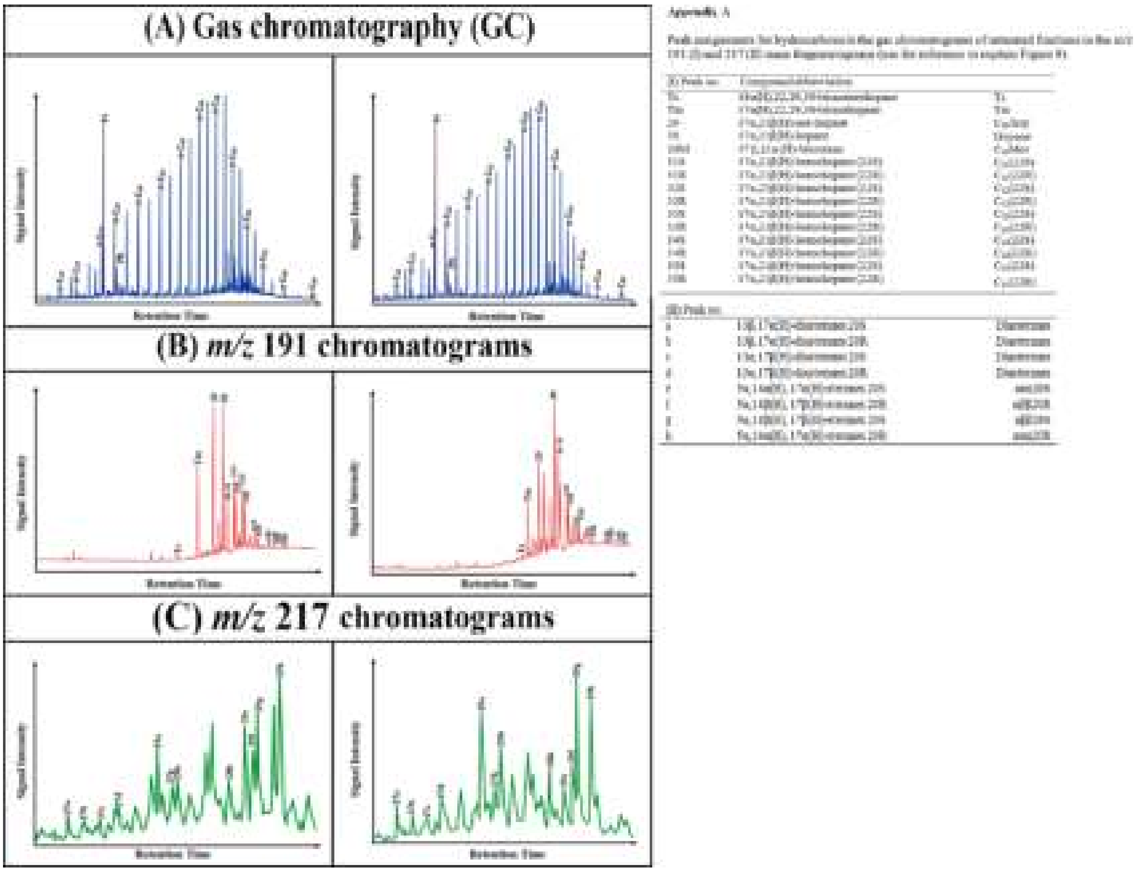

Figure 6. (A) Gas chromatograms, (B) m/z 191, and (C) m/z 217 mass fragmentograms of the aliphatic hydrocarbon fraction in the analyzed two organic-rich shale samples of the Mukalla Formation in the studied wells.

samples show OI values of less than 100 mg CO_2/g TOC (12−99), whereas other few samples show the highest OI values between 105 and 188 mg CO_2/g TOC (Table 1).

4.3. Biomarker Distributions. In the current study, the biomarker distribution of normal alkanes, isoprenoids, hopanoids, terpanes, and steranes of aliphatic HC fraction in the extracted Mukalla organic-rich shale samples was assessed using GC chromatography and CG-MS mass fragmentograms (Figure 6).

The gas chromatography of the studied shale samples comprises mainly of a series of n-C_{13} to n-C_{38} n-alkanes and is dominated by medium to high-molecular-weight homologues (n-C_{18} to n-C_{31}) (Figure 6a). Medium-molecular-weight (MMW) n-alkanes (C_{18} to C_{22}) are present in subordinate abundance while high-molecular-weight alkanes (>n-C_{23}) are present in high concentration (Figure 6a). In this normal alkane's distribution, the calculated carbon preference index (CPI), waxiness degree (WI), and terrigenous/aquatic ratio (TAR) were found to be in the range of 1.22−2.35, 3.20−5.33, and 4.05−6.00, respectively (Table 2).

The GC chromatograms also indicated the existence of pristane (Pr) and phytane (Ph) in the acyclic isoprenoid-examined samples as well (Figure 6a). The examined samples exhibit higher Pr when compared to Ph (Figure 6a), resulting in a higher Pr/Ph ratio of more than 3 (3.82 < Pr/Ph < 7.46) (Table 2). Moreover, the isoprenoids when compared to n-alkane concentrations (C_{17}−C_{18}) result in the Pr/n-C_{17} and Ph/n-C_{18} ratios varying from 2.47 to 8.20 and from 0.42 to 1.28, respectively (Table 2).

The m/z 191 chromatograms of two shale samples detected the presence of hopanoid and terpanes biomarkers (Figure 6b). In the examined shale samples, hopanoids are abundant and characterized by abundant C_{30} hopanes, C_{29} norhopanes, and homohopanes of C_{31}−C_{35} (Figure 6b). C_{30} hopane is the dominant hopanoid, followed by C_{29} norhopanes (Figure 6b), resulting in a C_{29}/C_{30} ratio between 0.62 and 0.95 (Table 2). The observed lower hopane C_{29}/C_{30} ratio of less than 1 indicates clay-rich facies.[41] The C_{30} hopane also dominates relative to the C_{31}R homohopane (Figure 6b), with a relatively low $C_{31}R/C_{30}$ ranging from 0.23 to 0.24 (Table 2).

One of the prominent features is the presence of C_{27} 18α (H)-22, 29, 30-trisnorneohopane (Ts), and C_{27} 17α (H)-22, 29, 30-trisnorhopane (Tm) in the m/z 191 mass fragmentogram (Figure 6b). The m/z 191 data exhibited significant quantities of C_{27} 17α (H)-22, 29, 30-trisnorhopane (Tm), with high Tm/Ts ratio in the range of 7.71−13.12 (Table 2). Moreover, several biomarker maturity ratios of the hopanes in the m/z 191 mass fragmentogram, specifically 22S/(22S + 22R) in C_{32} homohopane and C_{30} moretane/C_{30} hopane (CM_{30}/C_{30}), were calculated and are shown in Table 2.

Steranes and diasteranes are observed to be the most prominent compounds found in the m/z 217 mass fragmentogram of the saturated HCs (Figure 6c). In general, as compared to the abundance of diasteranes, mass fragmentograms of m/z 217 show a significant abundance of steranes (Figure 6c). In accordance with the steroid distributions, the C_{27}−C_{29} regular steranes consist of majorly C_{29} regular sterane, along with minor amounts of C_{28} and C_{27} regular steranes (Figure 6c), resulting in the relative percentages in the range of 16.66−17.27% C_{27},

https://doi.org/10.1021/acsomega.3c03691
ACS Omega 2023, 8, 30483−30499

Table 2. Biomarker Ratios and Carbon Stable Isotope ($\delta^{13}C$) of the Representative Organic-Rich Shales of the Mukalla Formation from Two Exploration Wells (Al-Furt-01 and Al-Jeza-01) in the Onshore Jiza-Qamar Basin, Eastern Yemen, Illustrating Source Organic Matter, Depositional Environment Conditions and Thermal Maturity[a]

		biomarker indicators of source organic matter and depositional environment conditions																biomarker indicators of thermal maturity				
		carbon stable isotope ($\delta^{13}C$ ‰)		normal alkanes, isoprenoids (GC)						hopanoids (m/z 191 ion)			steranes (m/z 217 ion)				hopanoids (m/z 191 ion)			steranes (m/z 217 ion)	
well	depth (m)	$\delta^{13}C$ ‰saturate	$\delta^{13}C$ ‰ aromatic	Pr/Ph	Pr/C_{17}	Ph/C_{18}	CPI	WI	TAR	Tm/Ts	C_{29}/C_{30}	HCR_{31}/HC_{30}	C_{27}/C_{29} regular steranes	regular steranes (%) C_{27}	C_{28}	C_{29}	Ts/Tm	M_{30}/C_{30}	C_{32} 22S/(22S + 22R)	C_{29} 20S/(20S + 20R)	C_{29} $\beta\beta/(\beta\beta + \alpha\alpha)$
Al-Furt-01	1203			3.82	2.47	0.65	2.35	3.20	4.86												
Al-Jeza-01	2142	−26.7	−26.0	6.47	8.70	1.28	2.04	4.65	6.00	13.12	0.95	0.23	0.32	17.27	28.08	54.66	0.08	0.64	0.43	0.24	0.32
	2814	−26.1	−27.6	6.06	4.42	0.52	1.22	4.58	4.36	7.71	0.62	0.24	0.26	16.66	20.22	63.12	0.13	0.35	0.52	0.40	0.40
	2826			7.46	4.31	0.42	1.29	5.33	4.05												

[a]Pr = pristane; Ph = phytane; CPI = carbon preference index (1): $\{2(C_{23} + C_{25} + C_{27} + C_{29})/(C_{22} + 2[C_{24} + C_{26} + C_{28}] + C_{30})\}$; waxiness degree (WI) = Σ (n-C21−n-C31)/Σ (n-C15−n-C20); TAR = terrigenous/aquatic ratio; C_{29}/C_{30} = C_{29} norhopane/C_{30} hopane; Ts = (C_{27} 18α (H)-22, 29, 30-trisnorneohopane); Tm = (C_{27} 17α (H)-22, 29, 30-trisnorhopane); and HCR_{31}/HC_{30} = C_{31} regular homohopane/C_{30} hopane, (CM_{30}/C_{30}) = C_{30} moretane/C_{30} hopane.

20.22−28.08% C_{28}, and 54.66−63.12% C_{29} regular steranes (Table 2). The standard sterane ratios such as C_{27}/C_{29} regular 20S/(20S + 20R) and $\beta\beta/(\beta\beta + \alpha\alpha)$ were further calculated (for more information, see Table 2).

4.4. Carbon Stable Isotope ($\delta^{13}C$). Bulk stable $\delta^{13}C$ analysis was executed on the aliphatic and aromatic hydrocarbon fractions from the two examined Mukalla shale samples in the studied one well. The isotope compositions of the studied shales show that the carbon ($\delta^{13}C$) of the aliphatic and aromatic HCs ranges from −26.1 to −26.7‰ and from −26.0 to −27.6‰, respectively (Table 2).

Sofer[39] and Summons et al.[42] reported that the $\delta^{13}C$ values mentioned above are a means to distinguish terrestrial from the marine OM input. Low $\delta^{13}C$ of heaver values (less negative) suggest a terrigenous origin, while high and moderate of lighter $\delta^{13}C$ values (more negative) come from marine OM (i.e., algae and microbes).[39] As a result, the examined shale samples appear to be receiving high contributions from the terrigenous OM, as evidenced by the low $\delta^{13}C$ values (Table 2). The finding of considerable concentration of terrigenous OM is supported by the Sofer diagram of the saturated ($\delta^{13}C_{sat.}$) and aromatic $\delta^{13}C_{Aro.}$) isotopic composition (Figure 7).

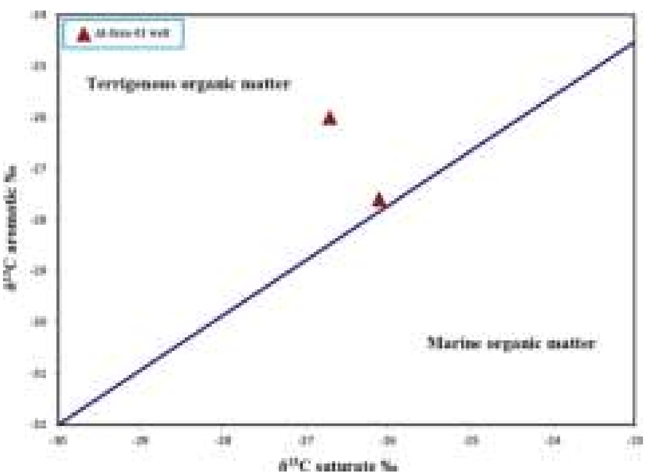

Figure 7. Sofer plot of $\delta^{13}C_{aro}$versus $\delta^{13}C_{sat}$ for two extracted Mukalla shale samples in the studied Al-Jeza well.

5. DISCUSSION

5.1. Organic Matter Input and Sedimentary Environmental Conditions. The OM input to the Mukalla shale interval, its origin, and source were assessed by employing biomarker results. The biomarker distributions together with and their ratios and parameters can accompany postulating logical interpretations related to the nature of OM input and paleoenvironmental deposition.[43−46]

The studied Mukalla shales show the bimodal distribution of the normal alkanes and isoprenoids, with abundant waxy alkanes (+n-C_{23}) and lower quantities of low-medium molecular compounds (n-C_{13}−n-C_{23}) (Figure 6a), indicating that the Mukalla shales were home to a mixture OM with high amounts of terrigenous OM input. As a biomodal distribution, the Mukalla shales have high CPI, WI, and TAR values (Table 2) and further indicate a dominant contribution of the land plant OM input (Figure 8).

However, the presence of high abundance of pristane compared to phytane, with high Pr/Ph of more than 3 employed

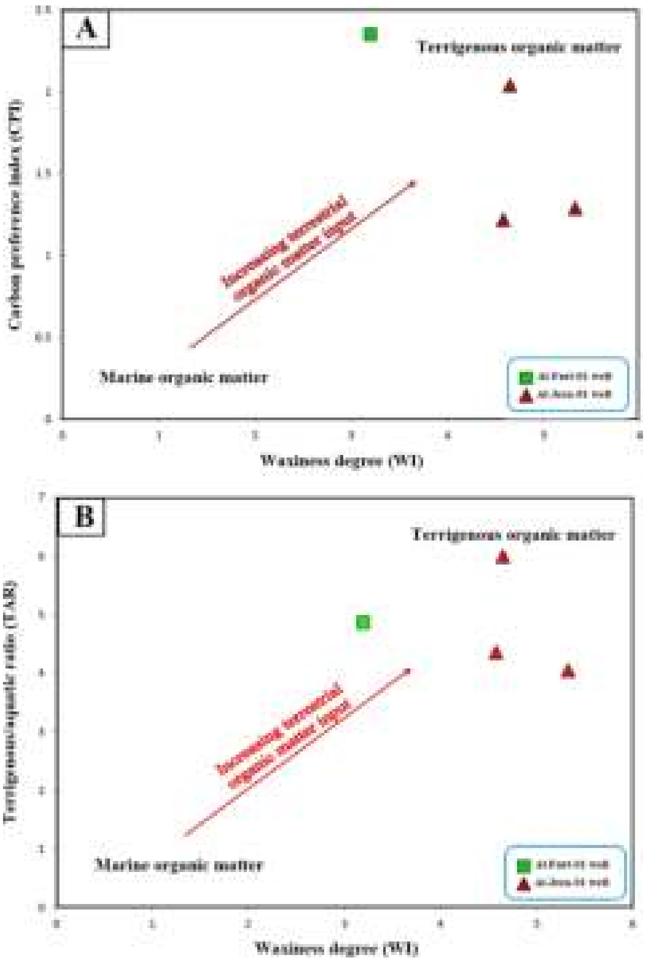

Figure 8. Geochemical biomarker results of the analyzed organic-rich shale samples showing (A) CPI versus waxiness degree (WI) and (B) terrigenous/aquatic ratio (TAR) versus WI, indicating that these shale sediments contain mainly terrigenous OM.

to infer the high contributions of terrigenous OM deposited under oxic environmental conditions.[47,48] The finding of the considerable concentration of terrigenous OM and highly oxic environmental conditions also demonstrated by the isoprenoids was compared to *n*-alkane concentrations (C_{17}−C_{18}), as indicated from the Pr/*n*-C_{17} and Ph/*n*-C_{18} ratios (Figure 9a). This interpretation of the high contributions of the terrigenous OM input under oxic conditions is also reinforced by the hopanoid and sterane distributions over the *m*/*z* 191 and 217 mass fragmentograms (Figure 6b,c).

In the *m*/*z* 191, the C_{30} hopane dominates relative to the C_{31}R homohopane (Figure 6b), with a relatively low $C_{31}R/C_{30}$ ranging from 0.23 to 0.24 (Table 2), inferring a non-marine setting for the deposition of the shales, as values more than 0.25 demonstrate marine depositional environment.[49] This interpretation is corroborated by the association between the $C_{31}R/C_{30}$ hopane and Pr/Ph ratios and indicates that the Mukalla shales were deposited in fluvial to fluvial deltaic depositional environments under highly oxic conditions (Figure 9b).

The elevated abundance of the Tm relates to the Ts (Figure 6b), with high Tm/Ts ratio of all the examined shale samples (Table 2), supporting the interpretation of the fact that these shale sediments received high contributions of terrigenous OM input.[50,51] The higher C_{29} regular sterane than C_{27} and C_{28} regular steranes (Figure 6c and Table 2) also supports the

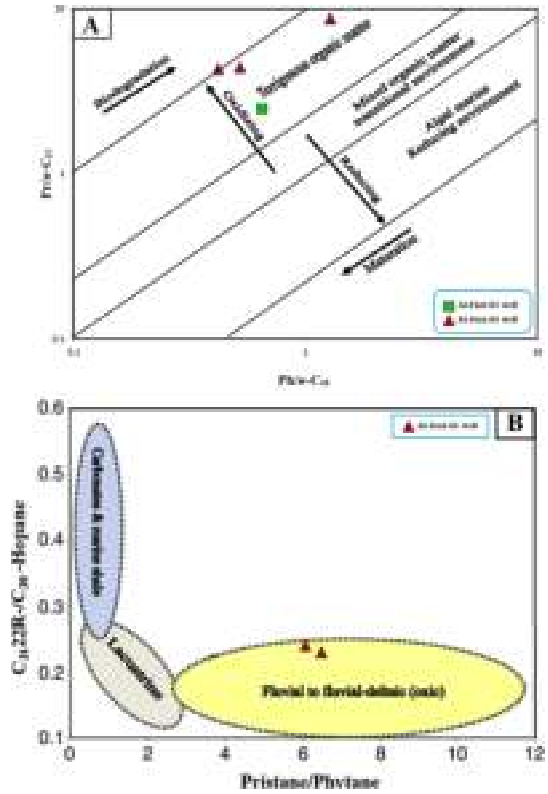

Figure 9. Geochemical biomarker results of the analyzed organic-rich shale samples showing (A) pristane/*n*-C_{17} versus phytane/*n*-C_{18} and (B) Pr/Ph versus C_{31} regular homohopane/C_{30} hopane (HCR_{31}/HC_{30}), indicating that these shale sediments contain mainly terrigenous OM and were deposited in fluvial to fluvial-deltaic environments under highly oxic conditions.

inference of primarily OM derived from land plants based on the adapted ternary diagram of Huang and Meinschein,[52] as shown in Figure 10. In addition, the higher abundance of the land plant OM input was also assessed by a low C_{27}/C_{29} regular sterane ratio (Figure 11).

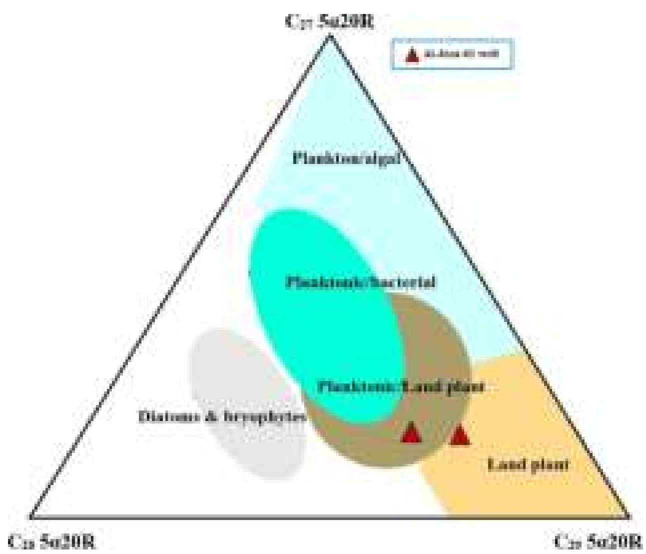

Figure 10. Ternary diagram of regular steranes (C_{27}−C_{29}) in the aliphatic hydrocarbon fraction in the analyzed organic-rich shale samples.

https://doi.org/10.1021/acsomega.3c03691
ACS Omega 2023, 8, 30483−30499

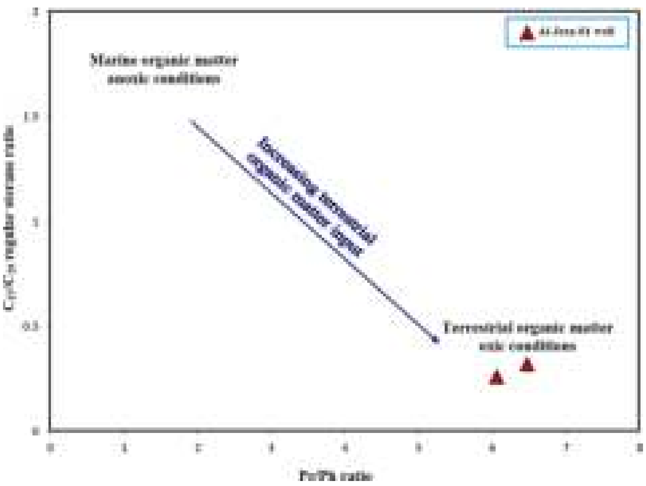

Figure 11. Geochemical biomarker results of the C_{27}/C_{28} regular steranes versus Pr/Ph ratio, indicating OM derived primarily from higher land plant OM and deposited under highly oxic conditions.

Moreover, the biomarker measurements are in compatibility together with the microscopic examination of the Mukalla shale samples. In this case, the high abundance of the land plant OM input to the Mukalla shale sediments is consistent with the observation of predominantly vitrinite maceral of up to 100% (Table 1). The vitrinite assemblages are mainly non-marine in origin (i.e., fluvial to fluvial deltaic environments) and were deposited under oxic environmental conditions.

5.2. Source Rock Characteristics and Implications for Hydrocarbon Exploration and Development. The source rock characteristics and efficacy of the hydrocarbon generation of the studied shale intervals of the Mukalla Formation from three exploration wells drilled in the onshore Jiza-Qamar Basin were discussed based on multi-geochemical results and microscopic features of the organic facies. However, extensive research on the successful exploration basins of unconventional and conventional petroleum resources, especially organic-rich sediments, indicates that OM abundance, OM type, maturity, and generation potential are worth considering.[1,3] Most studies have considered shale sediments with TOC > 2 wt % as high-quality source rocks.[53,54] However, the TOC content is conventionally reported as a function of weight percent, and it indicates the OM quantity in the sediments and their capacity for petroleum generation on thermal maturation.[53]

In terms of the TOC content, the high TOC values are represented for most of the analyzed Mukalla shale samples in the onshore Jiza-Qamar Basin with values >1 wt % and up to 19.48 wt % (Table 1), indicating a good source rock characteristics and ranking from good to very good hydrocarbon generation potential based on the association between the TOCs and thermal cracking of kerogen (S_2) values obtained by Rock-Eval pyrolysis (Figure 12a). However, the higher TOCs than S_2 yields (Table 1) also suggest the inference of primarily Type III and IV kerogen derived from land plants based on the adapted cross-plot of Langford and Blanc-Valleron[55] (1990), as seen in Figure 12b.

The interpretation of high contribution of hydrogen-poor kerogen is also inferred by the programmed pyrolysis results. The pyrolysis HI results are employed to recognize the bulk kerogen types.[56] Hear, the studied organic-rich shale horizons of the Mukalla Formation under consideration contain mainly Types III and IV kerogen, with minor contributions of mixed

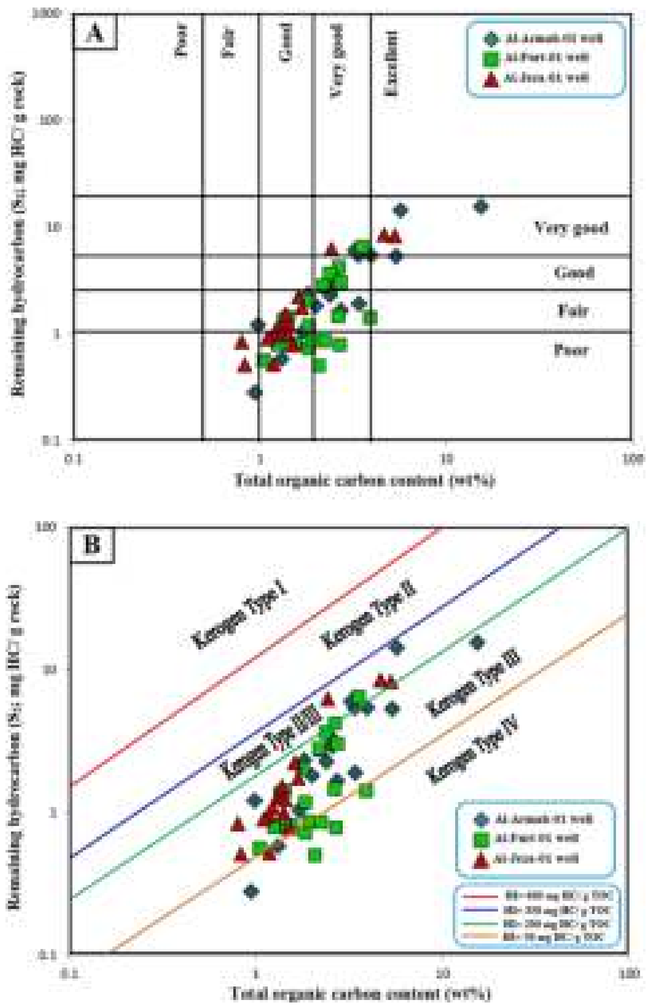

Figure 12. Geochemical correlations between the TOC content and Rock-Eval pyrolysis (S_2) for the analyzed organic-rich shale samples of the Mukalla Formation in the studied wells, showing that (A) these shales range from good to very petroleum generation potential and (B) contain mainly Type III and IV, with minor Type II/III kerogens.

III/II kerogen, as indicated when the HI and OI parameters were plotted on the Van-Krevelen kerogen-type diagrams (Figure 13a). The high contributions of the hydrogen-poor Types III and IV kerogen corroborate well with the T_{max} vs HI cross-plot (Figure 13b). By evaluating the bulk kerogen, it is evident that these shales are mainly gas-prone source rocks, as implied from the cross-plot of the TOC and HI geochemical data (Figure 14).

In addition, the sedimentary environment is an important factor in controlling the quality of the source rocks and hydrocarbon potential. In this regard, the fluvial, deltaic environment with a highly oxic and high deposition rate of the studied shales (Figure 9) would be beneficial for the formation of laminated or intercalated coaly sediments and shale layered structures, favoring land plant-derived OM abundant in hydrogen-poor kerogen (Figures 8, 10, and 11). The high contribution of hydrogen-poor Type III kerogen from the studied Mukalla shales is also confirmed by the high proportion of vitrinite maceral, as seen in the ternary diagram of Cornford[57] 16 (Figure 15a). The high abundance of vitrinite maceral also suggests that the shale intervals of the Mukalla Formation are mainly considered to be gas-prone source rocks, as indicated

https://doi.org/10.1021/acsomega.3c03691
ACS Omega 2023, 8, 30483−30499

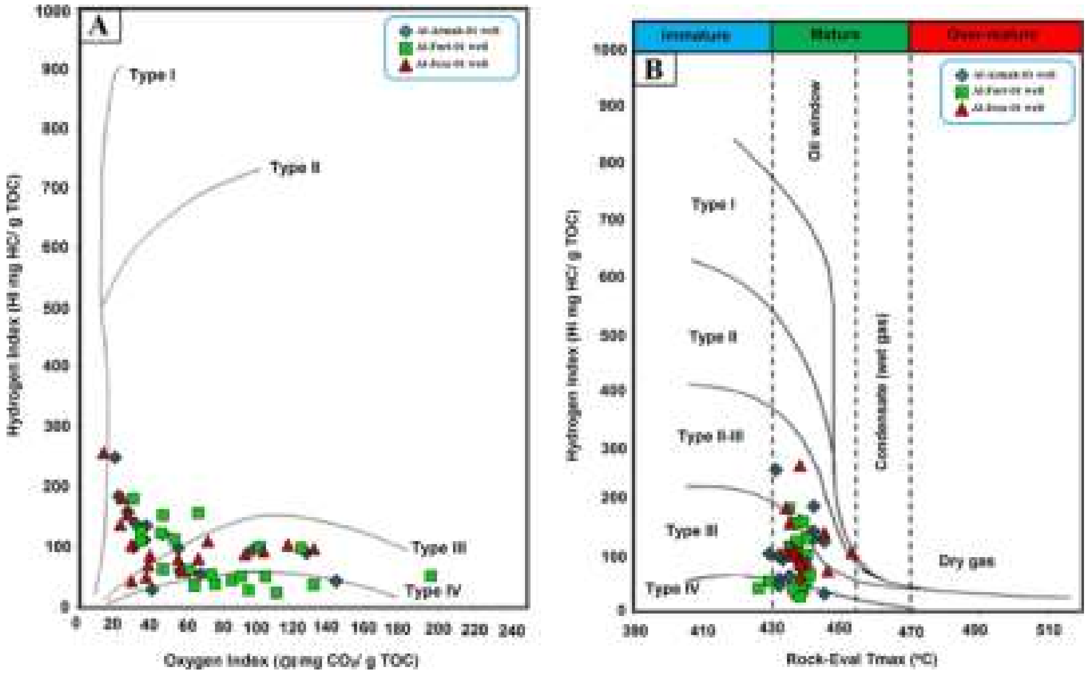

Figure 13. Chemical characteristics of kerogen of the organic-rich shale samples of the Mukalla Formation in the studied wells based on (A) hydrogen index (HI) versus oxygen index (OI) and (B) HI versus T_{max}, showing hydrogen-poor kerogen (III–II, III, and IV).

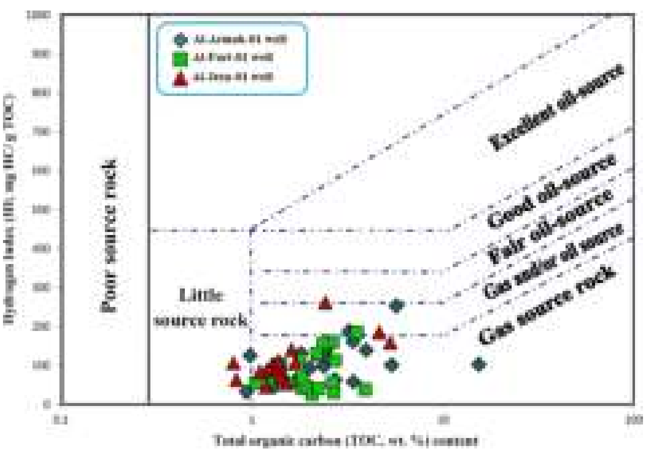

Figure 14. Geochemical correlations between the TOC content and Rock-Eval data (HI), implying that the analyzed Mukalla shale samples are both oil- and gas-prone source rocks, with high gas generation potential.

when the maceral composition is plotted on the Cornford's ternary diagram (Figure 15b).

Besides, the hydrocarbon generation capacity of the analyzed shale samples in the studied wells was further assessed for thermal maturity using several thermal maturation indicators, including % VRo, Rock-Eval pyrolysis (T_{max} and PI) data.

The VR measurements are the best indicator in providing valuable information about the organic maturation and evolution of the petroleum generation capacity.[58,59] In our case, the Mukalla shale samples from the studied wells have different thermal maturity stage, ranging from immature to very early mature oil generation window, as seen in Figure 4. However, the T_{max} and PI values confirm the previous thermal maturity level obtained from VR results. The T_{max} values show that the examined organic-rich shale samples are in low thermally mature and have entered immature to early mature oil generation window (Figure 13b). Moreover, the PI values were also evaluated through Rock Eval (RE) pyrolysis (S_1 and S_2), ranging between 0.04 and 0.31 (as shown in Table 1). This also agrees that the analyzed shales fall within the immature to early mature of oil window, as implicated by the relationship between PI and T_{max} (Figure 16).

The maturity degree of the Mukalla shale samples from the studied wells was also assessed using maturity-sensitive biomarker parameters of the *n*-alkane together with hopane and sterane biomarker data.[60−67] An estimate of the source rocks' maturity level can be derived from the *n*-alkane distribution in terms of CPI.[60,61] In this case, CPI values decrease from approximately 1.5 in immature source rocks to less than 1 in mature source rocks.[60] The CPI values obtained for the analyzed shales range from 1.22 to 2.35 (Table 2), indicating immature to early mature source rock.

In addition, the hopanes and steranes in the *m/z* 191 and 217 mass fragmentograms, specifically 22S/(22S + 22R) in C_{32} homohopanes, C_{30} moretane/C_{30} hopane (CM_{30}/C_{30}), and C_{29} sterane ratios of the 20S/(20S + 20R) and $\beta\beta/(\beta\beta + \alpha\alpha)$ (Table 2) also demonstrated the most accurate indications of biomarker maturity.[62−65]

The distribution of the C_{32}-homohopane is used to determine the [22S/(22S 22R)] isomerization ratio. As thermal maturity grows, this ratio reaches a maximum of 0.70.[64] The source rock is considered immature if the C_{32} ratio falls below 0.50. The source rocks with early mature to peak oil window have C_{32} ratios of 0.50 to 0.58, while an equilibrium point larger than 0.58 indicates further maturation phases.[64] Following this scale, the examined shales have different thermal maturity level, ranging from immature to the early mature oil generation phase, as demonstrated by the C_{32} hopane ratios between 0.43 and 0.52 (Table 2). It is also important to note that the ratios of the C_{29} steranes 20S/(20S + 20R) and $\beta\beta/(\beta\beta + \alpha\alpha)$ show the source rock' thermal maturity.[62−65] The oil window has reached if these ratios are more than 0.30 and 0.40.[66,67] Mukalla shale samples in

https://doi.org/10.1021/acsomega.3c03691
ACS Omega 2023, 8, 30483−30499

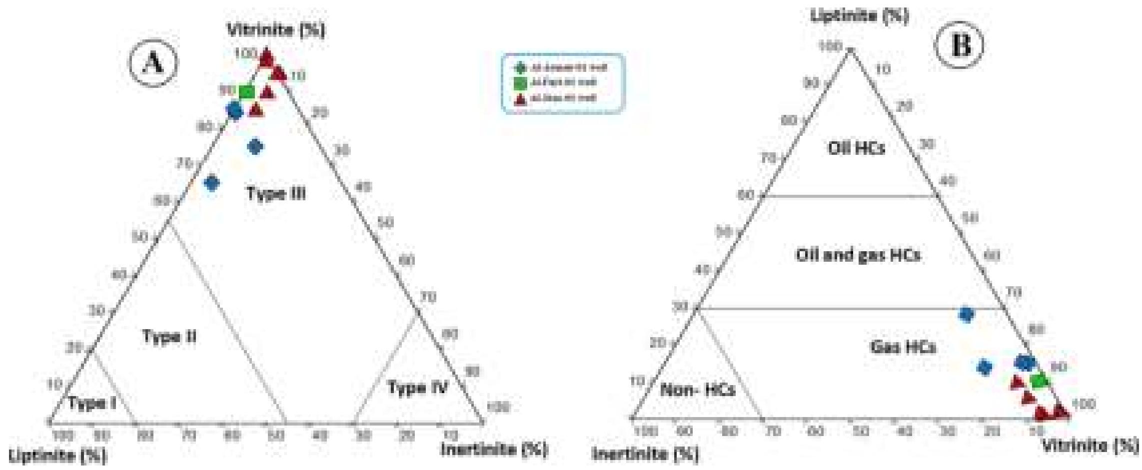

Figure 15. Ternary diagrams on the relative percentage of maceral types show that (A) analyzed shale samples are dominated by hydrogen-poor Type III kerogen and (B) analyzed shale samples can generate mainly gas HC.

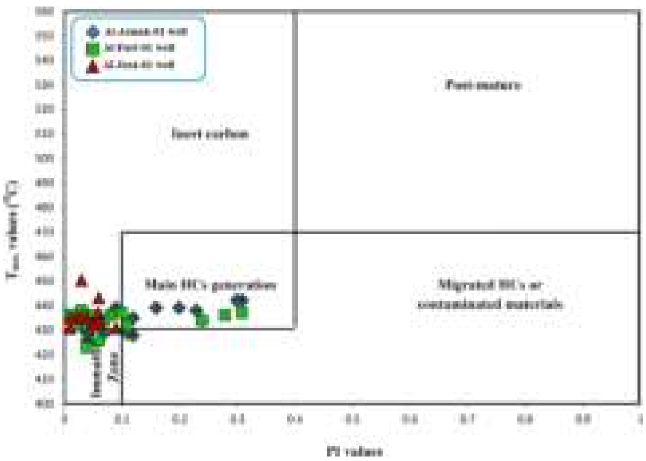

Figure 16. Relationship between thermal maturity indicators of T_{max} and PI for the analyzed organic-rich shale samples of the Mukalla Formation in the studied wells, showing immature to early mature maturity zones.

this study have 20S/(20S + 20R) and $\beta\beta/(\beta\beta + \alpha\alpha)$ C_{29} sterane ratios in the range of 0.24−0.40 and 0.32−0.40, respectively (Table 2), which further suggested immature to early mature source rocks (Figure 17a). This interpretation of the low thermal maturity for the Mukalla shale samples in the studied wells is also confirmed by combining the C_{32} hopane and C_{29} sterane $\beta\beta/(\beta\beta + \alpha\alpha)$ ratios (Figure 17b).

The CM_{30}/C_{30} ratios obtained from the mass fragmentograms of the m/z 191 are consistent with this maturation interpretation. As maturity increases, CM_{30}/C_{30} ratios decrease from approximately 0.8 in immature source rocks to less than 0.15 in mature source rocks, according to Mackenzie et al.[65] The relatively high CM_{30}/C_{30} ratios of the analyzed shale samples between 0.35 and 0.64 (Table 2) indicate low mature source rocks. The Ts/Tm ratio with the CM_{30}/C_{30} ratio also suggests different maturity levels of the shale samples in the studied wells (Figure 16c).

These biomarker maturity results are consistent with the previously maturity data of VRo, T_{max} and PI, as seen in Figures 4 and 16, and reveal that the OM (mainly hydrogen-poor kerogen) in the shale intervals of the Mukalla Formation from the studied wells in the onshore Jiza-Qamar reached low maturity level of the oil generation window and the commercial quantities of gas are yet to be generated. However, the maturity level of the studied shale section in the studied wells is vertically increased with the burial depth (Figure 4), and this is probably due to the burial temperature distributions. Therefore, the geothermal gradient through the burial depth is the critical factor that significantly affects the thermal maturity of the Mukalla source rock system and must be taken into account during development and hydrocarbon exploration through the Jiza-Qamar Basin.

However, because of tectonics, paleogeography, and paleoenvironmental deposition, the Mukalla Formation is equivalent throughout the Jiza-Qamar Basin in many ways. The primary difference between the Mukalla Formation across the Jiza-Qamar Basin (including this research) is connected to burial depths. As one goes through the Jiza-Qamar, the Mukalla Formation reached relatively shallow burial depths between 750 and 2840 m in the onshore part of the basin (Figure 3) and from 3100 to 4750 m in the offshore part of the basin.[7] This indicates that the Mukalla organic-rich shale source rock system in the deeper stratigraphic succession in the offshore Qamar-Jiza Basin likely achieved substantially high levels of thermal maturity because of burial temperatures and can be considered as a suitable candidate for producing commercial amounts of gas in the basin's offshore regions.

6. CONCLUSIONS

Organic-rich shale samples of the Late Cretaceous Mukalla Formation taken from three exploration wells in the onshore Jiza-Qamar Basin, Yemen were geochemically analyzed and utilized to define their OM characteristics and ability for potential of gas generation. Biomarker measurements together with carbon isotopic compositions were also utilized to assess the origin and source OM input and environmental conditions during the deposition of the Mukalla shale sediments.

The study's findings are summarized below.

- The shale samples from the studied wells are good to excellent source rocks capable of generating hydrocarbons based on their OM content, in which they have high TOC values of more than 1 wt % and up to 19.48 wt %.
- Geochemical characteristics together with microscopic investigation reveal that the studied Mukalla shales contain mainly hydrogen-poor Types III and IV kerogen and small amounts of mixed III/II kerogen, with HI values

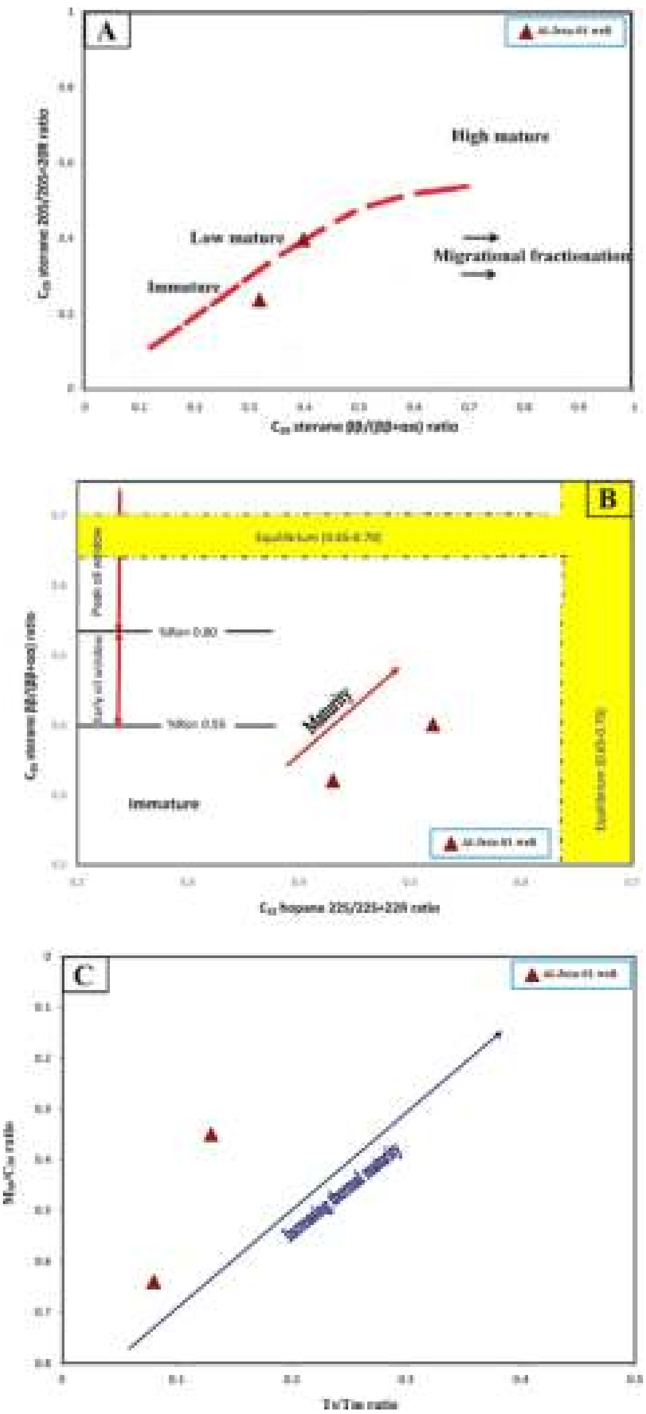

Figure 17. Geochemical cross-plot of the maturity−biomarker parameters the analyzed organic-rich shale samples showing (A) C_{29} sterane 20S/(20S + 20R) versus $\beta\beta/(\beta\beta + \alpha\alpha)$, (B) C_{32} hopane 22S/(22S + 22R) versus C_{29} sterane $\beta\beta/(\beta\beta + \alpha\alpha)$, and (C) Ts/Tm versus CM_{30}/C_{30}, showing immature to early mature oil generation window.

between 24 and 259 mg HC/g TOC; thus, they can generate mainly gas.

- Different biomarker ratios together with carbon ($\delta^{13}C$) isotopic values in cross-plots reveal that the studied shales contain the OM derived primarily from terrigenous land plants and deposited in fluvial to fluvial deltaic environments under highly oxic conditions. The characteristics of the high contributions of terrigenous OM are in agreement with the abundance of vitrinite maceral as established via a microscope.
- Using biomarker maturity indicators, the Mukalla shales in the studied wells from the onshore Qamar-Jiza Basin reached shallow burial depths, having low thermal maturity degree, comparable to the immature to early mature of the oil window stage. Therefore, they have not yet generated commercial amounts of hydrocarbon.
- This study can serve as a foundation for future hydrocarbon exploration in the deeper structural units of the offshore Qamar-Jiza Basin, where the Late Cretaceous Mukalla Formation has reached the high maturity level of the gas generation window and could release commercial amounts of gas.

APPENDIX A

Peak assignments for hydrocarbons in the gas chromatograms of saturated fractions in the m/z 191 (I) and 217 (II) mass fragmentograms (Table 3) (use for reference to explain Figure 9).

Table 3. Peak Assignments

(I) Peak no.	Compound abbreviation	
Ts	18α(H),22,29,30-trisnorneohopane	Ts
Tm	17α(H),22,29,30-trisnorhopane	Tm
29	$17\alpha,21\beta$(H)-nor-hopane	C29 hop
30	$17\alpha,21\beta$(H)-hopane	Hopane
30M	$17\beta,21\alpha$ (H)-Moretane	C30Mor
31S	$17\alpha,21\beta$(H)-homohopane (22S)	C31(22S)
31R	$17\alpha,21\beta$(H)-homohopane (22R)	C31(22R)
32S	$17\alpha,21\beta$(H)-homohopane (22S)	C32(22S)
32R	$17\alpha,21\beta$(H)-homohopane (22R)	C32(22R)
33S	$17\alpha,21\beta$(H)-homohopane (22S)	C33(22S)
33R	$17\alpha,21\beta$(H)-homohopane (22R)	C33(22R)
34S	$17\alpha,21\beta$(H)-homohopane (22S)	C34(22S)
34R	$17\alpha,21\beta$(H)-homohopane (22R)	C34(22R)
35S	$17\alpha,21\beta$(H)-homohopane (22S)	C35(22S)
35R	$17\alpha,21\beta$(H)-homohopane (22R)	C35(22R)
(II) Peak no.		
a	$13\beta,17\alpha$(H)-diasteranes 20S	Diasteranes
b	$13\beta,17\alpha$(H)-diasteranes 20R	Diasteranes
c	$13\alpha,17\beta$(H)-diasteranes 20S	Diasteranes
d	$13\alpha,17\beta$(H)-diasteranes 20R	Diasteranes
e	$5\alpha,14\alpha$(H), 17α(H)-steranes 20S	$\alpha\alpha\alpha$20S
f	$5\alpha,14\beta$(H), 17α(H)-steranes 20R	$\alpha\beta\beta$20R
g	$5\alpha,14\beta$(H), 17α(H)-steranes 20S	$\alpha\beta\beta$20S
h	$5\alpha,14\alpha$(H), 17α(H)-steranes 20R	$\alpha\alpha\alpha$20R

AUTHOR INFORMATION

Corresponding Authors

Mohammed Hail Hakimi − *Geology Department, Faculty of Applied Science, Taiz University, Taiz 6803, Yemen;* orcid.org/0000-0002-3320-9690; Email: ibnalhakimi@yahoo.com

Afikah Rahim − *Department of Geotecnics & Transportation, Faculty of Civil Engineering, Universiti Teknologi Malaysia, Johor Bahru 81310, Malaysia*; Email: afikahrahim@utm.my

Authors

Ali Kahal − *Geology and Geophysics Department, College of Science, King Saud University, Riyadh 145111, Saudi Arabia*

https://doi.org/10.1021/acsomega.3c03691
ACS Omega 2023, 8, 30483−30499

Waqas Naseem − *Department of Geology, University of Poonch Rawalakot, Azad Jammu & Kashmir Rawalakot 12350, Pakistan*
Wedad Alsomid − *Geology Department, Faculty of Applied Science, Taiz University, Taiz 6803, Yemen*
Alia Al-Buraihi − *Geology Department, Faculty of Applied Science, Taiz University, Taiz 6803, Yemen*
Thoraia Alyousofi − *Geology Department, Faculty of Applied Science, Taiz University, Taiz 6803, Yemen*
Shuaib Alqahtani − *Geology Department, Faculty of Applied Science, Taiz University, Taiz 6803, Yemen*
Hesham AbdulAziz Alyousofi − *Geology Department, Faculty of Applied Science, Taiz University, Taiz 6803, Yemen*
Naira Magdy Lotfy − *Exploration Department, Egyptian Petroleum Research Institute (EPRI), Cairo 11727, Egypt*

Complete contact information is available at:
https://pubs.acs.org/10.1021/acsomega.3c03691

Notes

The authors declare no competing financial interest.

■ ACKNOWLEDGMENTS

The authors are grateful to the Petroleum Exploration and Production Authority (PEPA), Republic of Yemen for providing the data set of this work. The second coauthor extends his sincere appreciation to the Researchers Supporting Project number (PSPD2023R546) at King Saud University in Riyadh, Saudi Arabia.

■ REFERENCES

(1) Jarvie, D. M.; Hill, R. J.; Ruble, T. E.; Pollastro, R. M. Unconventional shale-gas systems: The Mississippian Barnett Shale of north-central Texas as one model for thermogenic shale-gas assessment. *Am. Assoc. Pet. Geol. Bull.* **2007**, *91*, 475−499.

(2) Sohail, G. M.; Radwan, A. E.; Mahmoud, M. A review of Pakistani shales for shale gas exploration and comparison to North American shale plays. *Energy Rep.* **2022**, *8*, 6423−6442.

(3) Hackley, P. C.; Ryder, R. T. Organic geochemistry and petrology of Devonian shale in eastern Ohio: Implications for petroleum systems assessment. *Am. Assoc. Pet. Geol. Bull.* **2021**, *105*, 543−573.

(4) Wilkins, R. W.; George, S. C. Coal as a source rock for oil: a review. *Int. J. Coal Geol.* **2002**, *50*, 317−361.

(5) Alaug, A. S.; Batten, D. J.; Ahmed, A. F. Organic geochemistry, palynofacies and petroleum potential of the Mukalla Formation (late Cretaceous), Block 16, eastern Yemen. *Mar. Pet. Geol.* **2013**, *46*, 67−91.

(6) Hakimi, M. H.; Abdullah, W. H.; Mustapha, K. A.; Adegoke, A. K. Petroleum generation modeling of the Late Cretaceous coals from the Jiza-Qamar Basin as infer by kerogen pyrolysis and bulk kinetics. *Fuel* **2015**, *154*, 24−34.

(7) Hakimi, M. H.; Alaug, A. S.; Ahmed, A. F.; Yahya, M. M. A.; El Nady, M. M.; Ismail, I. M. Simulating the timing of petroleum generation and expulsion from deltaic source rocks: Implications for Late Cretaceous petroleum system in the offshore Jiza-Qamar Basin, Eastern Yemen-shore Jiza-Qamar Basin, Eastern Yemen. *J. Pet. Sci. Eng.* **2018**, *170*, 620−642.

(8) Hakimi, M. H.; Kumar, A.; Singh, A. K.; Lashin, A.; Rahim, A.; Varfolomeev, M. A.; Yelwa, N. A.; Mustapha, K. A. Geochemistry and organic petrology of the bituminite shales from the Kapurdi mine, Rajasthan of NW India: implications for waxy oil generation potential. *J. Pet. Explor. Prod. Technol.* **2022**, *13*, 505−521.

(9) Abdullah, W. H.; Togunwa, O. S.; Makeen, Y. M.; Hakimi, M. H.; Mustapha, K. A.; Baharuddin, M. H.; Sia, S. G.; Tongkul, F. Hydrocarbon source potential of Eocene-Miocene sequence of western Sabah, Malaysia. *Mar. Pet. Geol.* **2017**, *83*, 345−361.

(10) Alizadeh, B.; Opera, A.; Kalani, M.; Alipour, M. Source rock and shale oil potential of the Pabdeh Formation (Middle-Late Eocene) in the Dezful Embayment, southwest Iran. *Geol. Acta* **2020**, *18*, 1−22.

(11) Hazra, B.; Wood, D. A.; Vishal, V.; Varma, A. K.; Sakha, D.; Singh, A. K. Porosity controls and fractal disposition of organic-rich Permian shales using low-pressure adsorption techniques. *Fuel* **2018**, *220*, 837−848.

(12) Singh, A. K.; Hakimi, M. H.; Kumar, A.; Ahmed, A.; Abidin, N. S. Z.; Kinawy, M.; Mahdy, O. E.; Lashin, A. Geochemical and organic petrographic characteristics of high bituminous shales from Gurha mine in Rajasthan, NW India. *Sci. Rep.* **2020**, *10*, 22108.

(13) Kumar, A.; Hakimi, M. H.; Singh, A. K.; Abdullah, W. H.; Zainal Abidin, N. S.; Rahim, A.; Mustapha, K. A.; Yelwa, N. A. Geochemical and Petrological Characterization of the Early Eocene Carbonaceous Shales: Implications for Oil and Gas Exploration in the Barmer Basin, Northwest India. *ACS Omega* **2022**, *7*, 42960−42974.

(14) Makeen, Y. M.; Abdullah, W. H.; Hakimi, M. H.; Mustapha, K. A. Source rock characteristics of the Lower Cretaceous Abu Gabra Formation in the Muglad Basin, Sudan, and its relevance to oil generation studies. *Mar. Petrol. Geol.* **2015**, *59*, 505−516.

(15) Makeen, Y. M.; Abdullah, W. H.; Abdul Ghofur, M. N.; Ayinla, H. A.; Hakimi, M. H.; Shan, X.; Mustapha, K. A.; Kamal Shuib, M.; Liang, Y.; Zainal Abidin, N. S. Hydrocarbon generation potential of Oligocene oil shale deposit at onshore Penyu Basin, Chenor, Pahang, Malaysia. *Energy Fuels* **2019**, *33*, 89−105.

(16) Hill, R. J.; Zhang, E.; Katz, B. J.; Tang, Y. Modeling of gas generation from the Barnett shale, Fort Worth Basin, Texas. *Am. Assoc. Pet. Geol. Bull.* **2007**, *91*, 501−521.

(17) Katz, B. J.; Lin, F. Consideration of the limitations of thermal maturity with respect to vitrinite reflectance, Tmax, and other proxies. *AAPG Bull.* **2021**, *105*, 695−720.

(18) Nie, H.; Jin, Z.; Li, P.; Jay Katz, B.; Dang, W.; Liu, Q.; Ding, J.; Jiang, S.; Li, D. Deep shale gas in the Ordovician-Silurian Wufeng−Longmaxi formations of the Sichuan Basin, SW China: Insights from reservoir characteristics, preservation conditions and development strategies. *J. Asian Earth Sci.* **2023**, *244*, 105521.

(19) Mahdi, A. Q.; Abdel-Fattah, M. I.; Radwan, A. E.; Hamdan, H. A. An integrated geochemical analysis, basin modeling, and palynofacies analysis for characterizing mixed organic-rich carbonate and shale rocks in Mesopotamian Basin, Iraq: Insights for multisource rocks evaluation. *J. Pet. Sci. Eng.* **2022**, *216*, 110832.

(20) Radwan, A. E.; Wood, D. A.; Mahmoud, M.; Tariq, Z. Gas adsorption and reserve estimation for conventional and unconventional gas resources. In *Sustainable Geoscience for Natural Gas Subsurface Systems*; Gulf Professional Publishing, 2022, pp 345−382.

(21) As-Saruri, M. A.; Sorkhabi, R.; Baraba, R. Sedimentary basins of Yemen: their tectonic development and lithostratigraphic cover. *Arabian J. Geosci.* **2010**, *3*, 515−527.

(22) Alaug, A. S. Hydrocarbon potential of the Upper Cretaceous succession at well 16/U-1, onshore Qamar Basin, eastern Yemen. *J. Pet. Geol.* **2011a**, *34*, 87−107.

(23) Alaug, A. S. Source rocks evaluation, hydrocarbon generation and palynofacies study of Late Cretaceous succession at 16/G-1 offshore well in Qamar Basin, eastern Yemen. *Arabian J. Geosci.* **2011b**, *4*, 551−566.

(24) Redfern, P.; Jones, J. A. The interior rifts of the Yemen: analysis of basin structure and stratigraphy in a regional plate tectonic context. *Basin Res.* **1995**, *7*, 337−356.

(25) Beydoun, Z. R.; Saruri, M. L.; El-Nakhal, H.; Al-Ganad, I. N.; Baraba, R. S.; Nani, A. O.; Al-Aawah, M. H. Republic of Yemen. International Lexicon of Stratigraphy. *IUGS Publication* **1998**, *3*, 245.

(26) Ellis, A. C.; Kerr, H. M.; Cornwell, C. P.; Williams, D. O. A tectonostratigraphic framework for Yemen and its implications for hydrocarbon potential. *Pet. Geosci.* **1996**, *2*, 29−42.

(27) Sharland, P. R.; Archer, R.; Cassey, D. M.; Davies, R. B.; Hall, S. H.; Heward, A. P.; Horbery, A. D.; Simmons, M. D. *Arabian Plate Sequence Stratigraphy*; Gulf PetroLink: Bahrain, 2001, p 371.

(28) Alaug, A. S.; Al-Wosabi, K. A.; Al-Ramsy, J. Evaluation of Late Jurassic source rocks, Al-Jawf Basin, NE central Yemen. *Bull. Tethys Geol. Soc.* **2008**, *3*, 99−110.

(29) Alaug, A. S.; Leythaeuser, D.; Bruns, B.; Ahmed, A. F. Source rock evaluation, modelling, maturation, and reservoir characterization of the block 18 oilfields, Sab'atayn Basin, Yemen. *Iranian J. Earth Sci.* **2011**, *3*, 134−152.

(30) Hakimi, M. H.; Abdullah, W. H.; Shalaby, M. R. Organic geochemical characteristics and depositional environments of the Jurassic shales in the Masila Basin of eastern Yemen. *GeoArabia* **2011a**, *16*, 47−64.

(31) Hakimi, M. H.; Abdullah, W. H.; Shalaby, M. R. Organic geochemical characteristics of crude oils from the Masila Basin, eastern Yemen. *Org. Geochem.* **2011b**, *42*, 465−476.

(32) Hakimi, M. H.; Abdullah, W. H. Source rock characteristics and hydrocarbon generation modelling of Upper Cretaceous Mukalla Formation in the Jiza-Qamar Basin, Eastern Yemen. *Mar. Pet. Geol.* **2014**, *51*, 100−116.

(33) Hakimi, M. H.; Abdullah, W. H. Source rock characteristics and hydrocarbon generation modelling of upper cretaceous Mukalla Formation in the Jiza-Qamar basin, eastern Yemen. *Mar. Petrol. Geol.* **2014**, *51*, 100−116.

(34) Hakimi, M. H.; Ahmed, A.; Kahal, A. Y.; Hersi, O. S.; Al Faifi, H. J.; Qaysi, S. Organic geochemistry and basin modeling of Late Cretaceous Harshiyat Formation in the onshore and offshore basins in Yemen: Implications for effective source rock potential and hydrocarbon generation. *Mar. Pet. Geol.* **2020**, *122*, 104701.

(35) Brannan, J.; Gerdes, K. D.; Newth, I. R. Tectono-stratigraphic development of the Qamar Basin, eastern Yemen. *Mar. Pet. Geol.* **1997**, *14*, 701,IN7−730,IN12.

(36) Espitalié, J.; La Porte, J. L.; Madec, M.; Marquis, F.; Le Plat, P.; Paulet, J.; Boutefeu, A. Méthode rapide de caractérisation des roches mètres, de leur potentiel pétrolier et de leur degré d'évolution. *Rev. Inst. Fr. Pet.* **1977**, *32*, 23−42.

(37) Lafargue, E.; Marquis, F.; Pillot, D. Rock-Eval 6 applications in hydrocarbon exploration, production, and soil contamination studies. *Rev. Inst. Fr. Pet.* **1998**, *53*, 421−437.

(38) Peters, K.; Cassa, M. Applied Source Rock Geochemistry. In *American Association of Petroleum Geologists*; Magoon, L. B., Dow, W. G., Eds.; *The petroleum system from source to trap*, 1994; Vol. *60*, pp 93−117.

(39) Sofer, Z. Stable carbon isotope compositions of crude oils: application to source depositional environments and petroleum alteration. *Am. Assoc. Petrol. Geol. Bull.* **1984**, *68*, 31−49.

(40) Taylor, G.; Teichmüller, M.; Davis, A.; Diessel, C. *Organic Petrology*; Schweizerbart'sche Verlagsbuchhandlung, 1998.

(41) Gürgey, K. Geochemical characteristics and thermal maturity of oils from the Thrace Basin (western Turkey) and western Turkmenistan. *J. Pet. Geol.* **1999**, *22*, 167−189.

(42) Summons, R. E.; Thomas, J.; Maxwell, J. R.; Boreham, C. J. Secular and environmental constraints on the occurrence of dinosterane in sediments. *Geochim. Cosmochim. Acta* **1992**, *56*, 2437−2444.

(43) Hadad, Y. T.; Hakimi, M. H.; Abdullah, W. H.; Kinawy, M.; El Mahdy, O.; Lashin, A. Organic geochemical characteristics of Zeit source rock from Red Sea Basin and their contribution to organic matter enrichment and hydrocarbon generation potential. *J. African Earth Sci.* **2021**, *177*, 104151.

(44) Murray, A. P.; Boreham, C. J. *Organic geochemistry in petroleum exploration: Canberra, Australia*; Australian Geological Survey Organization, 1992, p 230.

(45) Waples, D. W.; Machihara, T. Biomarkers for geologists: A practical guide to the application of steranes and triterpanes in petroleum geology. AAPG Methods in Exploration; American Association of Petroleum Geologists, 1991; Vol. *9*, p 91.

(46) Zumberge, J. E. Terpenoid biomarker distributions in low maturity crude oils. *Org. Geochem.* **1987**, *11*, 479−496.

(47) Didyk, B. M.; Simoneit, B. R. T.; Brassell, S. C.; Eglinton, G. Organic geochemical indicators of palaeoenvironmental conditions of sedimentation. *Nature* **1978**, *272*, 216−222.

(48) Chandra, K.; Mishra, C. S.; Samanta, U.; Gupta, A.; Mehrotra, K. L. Correlation of different maturity parameters in the Ahmedabad−Mehsana block of the Cambay basin. *Org. Geochem.* **1994**, *21*, 313−321.

(49) Peters, K. E., Walters, C. C., Moldowan, J. M. (2005). *The biomarker guide 2: Biomarkers and isotopes in petroleum exploration and Earth history*, 2d ed.: Cambridge, United Kingdom, Cambridge University Press, 704 p.

(50) Alias, F. L.; Abdullah, W. H.; Hakimi, M. H.; Azhar, M. H.; Kugler, R. L. Organic geochemical characteristics and depositional environment of the Tertiary Tanjong Formation coals in the Pinangah area, onshore Sabah, Malaysia. *Int. J. Coal Geol.* **2012**, *104*, 9−21.

(51) Sarki Yandoka, B. M.; Abdullah, W. H.; Abubakar, M. B.; Hakimi, M. H.; Mustapha, K. A.; Adegoke, A. K. Organic geochemical characteristics of Cretaceous Lamja Formation from Yola Sub-basin, Northern Benue Trough, NE Nigeria: implication for hydrocarbon-generating potential and paleodepositional setting. *Arabian J. Geosci.* **2015**, *8*, 7371−7386.

(52) Huang, W. Y.; Meinschein, W. G. Sterols as ecological indicators. *Geochem. Cosmochim. Acta* **1979**, *43*, 739−745.

(53) Peters, K. E. Guidelines for evaluating petroleum source rock using programmed pyrolysis. *Am. Assoc. Petrol. Geol. Bull.* **1986**, *70*, 318−329.

(54) Katz, B.; Lin, F. Lacustrine basin unconventional resource plays: key differences. *Mar. Pet. Geol.* **2014**, *56*, 255−265.

(55) Langford, F. F.; Blanc-Valleron, M. M. Interpreting Rock-Eval pyrolysis data using graphs of pyrolizable hydrocarbons versus total organic carbon. *Am. Assoc. Pet. Geol. Bull.* **1990**, *74*, 799−804.

(56) Mukhopadhyay, P. K.; Wade, J. A.; Kruge, M. A. Organic facies and maturation of Jurassic/Cretaceous rocks, and possible oil-source rock correlation based on pyrolysis of asphaltenes, Scotian Basin, Canada. *Canada Org. Geochem.* **1995**, *22*, 85−104.

(57) Cornford, C. Organic deposition at a continental rise; organic geochemical interpretations and synthesis at DSDP Site 397, eastern North Atlantic. *Init Repts Deep Sea Drilling Projects* **1979**, *47*, 503−510.

(58) Sweeney, J. J.; Burnham, A. K. Evaluation of a simple model of vitrinite reflectance based on chemical kinetics. *Am. Assoc. Petrol. Geol. Bull.* **1990**, *74*, 1559−1570.

(59) Teichmüller, M.; Littke, R.; Robert, P. Coalification and maturation. In *Organic petrology*; Taylor, G. H., Teichmüller, M., Davis, A., Diessel, C. F., Littke, R., Robert, P., Eds.; Gebrüder Borntraeger: Berlin, 1998, pp 86−174.

(60) Bray, E. E.; Evans, E. D. Distribution of n-paraffins as a clue to recognition of source beds. *Geochim. Cosmochim. Acta* **1961**, *22*, 2−15.

(61) Peters, K. E.; Moldowan, J. M. *The biomarker guide: Interpreting molecular fossils in petroleum and ancient sediments*; Prentice Hall: Englewood Cliffs, New Jersey, 1993, p 363.

(62) Seifert, W. K.; Moldowan, J. M. Paleo-reconstruction by biological markers. *Geochim. Cosmochim. Acta* **1981**, *45*, 783−794.

(63) Seifert, W. K.; Michael Moldowan, J. Applications of steranes, terpanes and monoaromatics to the maturation, migration and source of crude oils. *Geochim. Cosmochim. Acta* **1978**, *42*, 77−95.

(64) Seifert, W. K.; Moldowan, J. M. Use of biological markers in petroleum exploration. In *24, Methods in Geochemistry and Geophysics Book*; Johns, R. B., Ed.: Amsterdam Series, 1986, pp 261−290.

(65) Mackenzie, A. S.; Patience, R. L.; Maxwell, J. R.; Vandenbroucke, M.; Durand, B. Molecular parameters of maturation in the Toarcian shales, Paris Basin, France—I. Changes in the configurations of acyclic isoprenoid alkanes, steranes and triterpanes. *Geochim. Cosmochim. Acta* **1980**, *44*, 1709−1721.

(66) Gharib, A. F.; Özkan, A. M.; Hakimi, M. H.; Zainal Abidin, N.; Lashin, A. Integrated geochemical characterization and geological modeling of organic matter-rich limestones and oils from Ajeel Oilfield in Mesopotamian Basin, Northern Iraq. *Mar. Pet. Geol.* **2021**, *126*, 104930.

(67) Hakimi, M. H.; Abdullah, W. H.; Shalaby, M. R. Molecular composition and organic petrographic characterization of Madbi

source rocks from the Kharir Oilfield of the Masila Basin (Yemen): palaeoenvironmental and maturity interpretation. *Arabian J. Geosci.* **2012**, *5*, 817−831.

https://doi.org/10.1021/acsomega.3c03691
ACS Omega 2023, 8, 30483−30499